

Rapid reactions between CO2, brine and silicate minerals during geological carbon storage: Modelling based on a field CO2 injection experiment

Mike Bickle, Niko Kampman, Hazel Chapman, Chris Ballentine, Benoit Dubacq, Albert Galy, Tule Sirikitputtisak, Oliver Warr, Max Wigley, Zheng Zhou

▶ **To cite this version:**

Mike Bickle, Niko Kampman, Hazel Chapman, Chris Ballentine, Benoit Dubacq, et al.. Rapid reactions between CO2, brine and silicate minerals during geological carbon storage: Modelling based on a field CO2 injection experiment. Chemical Geology, 2017, 468, pp.17 - 31. 10.1016/j.chemgeo.2017.07.031 . insu-03218907

HAL Id: insu-03218907
https://insu.hal.science/insu-03218907

Submitted on 6 May 2021

HAL is a multi-disciplinary open access archive for the deposit and dissemination of scientific research documents, whether they are published or not. The documents may come from teaching and research institutions in France or abroad, or from public or private research centers.

L'archive ouverte pluridisciplinaire **HAL**, est destinée au dépôt et à la diffusion de documents scientifiques de niveau recherche, publiés ou non, émanant des établissements d'enseignement et de recherche français ou étrangers, des laboratoires publics ou privés.



Distributed under a Creative Commons Attribution - NoDerivatives 4.0 International License

Chemical Geology 468 (2017) 17–31

Contents lists available at ScienceDirect

Chemical Geology

journal homepage: www.elsevier.com/locate/chemgeo

Rapid reactions between CO_2, brine and silicate minerals during geological carbon storage: Modelling based on a field CO_2 injection experiment

Mike Bickle[a,*], Niko Kampman[a,b], Hazel Chapman[a], Chris Ballentine[c], Benoit Dubacq[a,d], Albert Galy[a,e], Tule Sirikitputtisak[f], Oliver Warr[g], Max Wigley[a], Zheng Zhou[h]

[a] Dept. Earth Sciences, Downing Street, Cambridge CB2 3EQ, UK
[b] Shell Global Solutions International, Kessler Park 1, 2288 GS Rijswijk, The Netherlands
[c] Department of Earth Sciences, South Parks Road, Oxford OX1 3AN, UK
[d] Sorbonne Universités, UPMC Univ. Paris 06, CNRS, Institut des Sciences de la Terre de Paris (ISTeP), 4 place Jussieu, 75005 Paris, France
[e] CRPG, Centre de Recherches Pétrologiques et Géochimiques, 15 rue Notre Dame des Pauvres, 54501 Vandoeuvre lès Nancy, France
[f] International Affairs and Cooperative Education, Prince of Songkla University, Surat Thani Campus, Thailand
[g] Department of Earth Sciences, Earth Sciences Centre, University of Toronto, Toronto, Ontario M5S 3B1, Canada
[h] Lancaster Environment Centre, Lancaster University, Lancaster LA1 4YQ, UK

ARTICLE INFO

Keywords:
Geological carbon storage
CO_2 injection experiment
Fluid-mineral reactions
Plagioclase dissolution rates
Enhanced oil recovery

ABSTRACT

The dissolution of CO_2 into formation brines and the subsequent reactions of the CO_2-charged brines with reservoir minerals are two key processes likely to increase the security of geological carbon-dioxide storage. These processes will be dependent on the permeability structure and mineral compositions of the reservoirs, but there is limited observational data on their rates. In this paper we report the cation and anion concentrations and Sr, oxygen and carbon isotopic compositions of formation waters from four extraction wells sampled at surface, over ~6 months after commencement of CO_2 injection in a five spot pattern for enhanced oil recovery at the Salt Creek field, Wyoming. Sampled fluids, separated from the minor oil component, exhibit near-monotonic increases in alkalinity and concentrations of cations but little change in Cl and Br concentrations and oxygen and deuterium isotope ratios. The increases in alkalinity are modelled in terms of reaction with reservoir calcite and silicate minerals as the changes in fluid chemistry and Sr-isotopic compositions are inconsistent with simple addition of injected fluids sampled over the course of the experiment. The reservoir mineral chemical and isotopic compositions are characterised by sampling core as well as surface exposures of the Frontier Formation elsewhere in Wyoming. The evolution of the fluid chemistries reflects extensive dissolution of both carbonate and silicate minerals over the course of the six months sampling implying rapid dissolution of CO_2 in the formation waters and reaction of CO_2-bearing brines with formation minerals. Rates of CO_2 diffusion into the brines and advection of CO_2 charged brines in the reservoir are sufficiently slow that, if present, calcite should react to be close to equilibrium with the fluids. This allows estimation of the CO_2 partial pressures in the sampled fluids and comparison with the thermodynamic driving force for the relatively rapid average plagioclase dissolution rates of $\sim 10^{-12}$ mol·m^{-2}·s^{-1}.

1. Introduction

Dissolution of CO_2 in formation brines and the consequent fluid-mineral reactions in reservoirs are potentially important processes which lead to the long-term security of geological carbon storage (IPCC, 2005; Benson and Cole, 2008; Bickle, 2009). However the rates and ultimate significance of these processes to storage security are poorly constrained. Dissolution of CO_2 increases brine densities and storage security, as the denser brines will not be subject to the buoyancy of the super-critical CO_2. However the volume of brine needed is 10 to 15 times that of the CO_2. The resulting reactions between the acid CO_2-charged brines and reservoir minerals may either increase or decrease storage security. Carbonate minerals in reservoirs will dissolve rapidly (Xu et al., 2007), which will buffer the fluid pH and may increase reservoir porosities slightly and permeabilities significantly. The acid CO_2-saturated brines may corrode caprocks or fault zones but this may be offset by the more sluggish reactions between brines and silicate minerals causing pH to rise and carbonate minerals to precipitate (Kampman et al., 2016). The latter may block fluid escape paths and store a fraction of the CO_2 in much more secure solid forms.

* Corresponding author.
E-mail address: mb72@esc.cam.ac.uk (M. Bickle).

http://dx.doi.org/10.1016/j.chemgeo.2017.07.031
Received 16 December 2016; Received in revised form 26 July 2017; Accepted 31 July 2017
Available online 02 August 2017
0009-2541/ © 2017 The Authors. Published by Elsevier B.V. This is an open access article under the CC BY license (http://creativecommons.org/licenses/BY/4.0/).

The key step in the CO_2-brine-mineral reactions is the rate at which the CO_2 dissolves in the brine. CO_2 diffusion in brine is sluggish with diffusion distances at most ~0.2 m in a year or ~1 m in ~30 years. However two processes in reservoirs may substantially increase the rate of CO_2 dissolution. In more permeable reservoirs the denser CO_2-saturated brine may sink setting up a convective circulation that cycles unsaturated brine against an overlying CO_2 plume. In favourable settings this may cause a significant fraction of the CO_2 to be dissolved within decades (e.g. Neufeld et al., 2010). The second mechanism relates to the innate heterogeneity of rocks. The well imaged CO_2 storage site at Sleipner demonstrates that the injected CO_2 flows by multiple paths and is trapped in multiple layers even in a relatively homogeneous reservoir (e.g. Boait et al., 2012). This increases the CO_2-brine surface area by at least an order-of-magnitude and probably much more, with a corresponding increase in CO_2 dissolution rates. Nearly all the porous sedimentary rocks which will comprise the CO_2 storage reservoirs are bedded on scales of ~1/3 m and have corresponding order-of-magnitude variations in their permeabilities. This, combined with the natural tendency of the less viscous CO_2 to finger when injected into more viscous brines (Saffman-Taylor instablity, Saffman and Taylor, 1958), will also cause substantial increases in brine-CO_2 contact areas and therefore CO_2 dissolution rates.

However it is difficult or impossible to predict a priori how fast CO_2 will dissolve in formation brines. One set of possible observations that indirectly reflect CO_2 dissolution rates is on the nature and rates of fluid-mineral reactions driven by the increases in dissolved CO_2 in formation brines. These necessarily need to be made in pilot-scale CO_2 injection experiments to reduce flow paths, time scales and allow adequate sampling of fluids. There have been a small number of such experiments (see review by Kampman et al., 2014) but determination of fluid-mineral reactions in these has either not been attempted, is restricted because sampling bore holes were swamped by the CO_2 plume within days, the formations contained unreactive quartz-rich lithologies or fluid composition data remains unpublished.

CO_2 injection for enhanced oil recovery provides opportunities to investigate the flow, dissolution and brine-CO_2 reactions in field settings analogous to likely CO_2 storage sites (e.g. Hovorka et al., 2011; Worden and Smith, 2004). The industrial exploitation injects substantial volumes of CO_2 and the continuous production allows time-series sampling of produced fluids from a distributed set of wells. Disadvantages include the presence of oil in the fluids and the oil fields often having been subject to a long history of exploitation involving previous water flooding. Further, fluids sampled from production wells at surface will have decompressed and exsolved CO_2 precluding direct measurement of dissolved CO_2 at reservoir conditions.

In this paper we calculate the nature and progress of fluid-mineral reactions from changes in the sampled fluid chemical and isotopic compositions based on sampling and analysing produced fluids from a CO_2 injection phase for enhanced oil recovery at a site in the Salt Creek Field, Wyoming. The CO_2 was injected into the ~20 m thick 2nd Wall Creek sandstone unit and produced fluids were sampled over a six month period after initiation of the CO_2 injection. The produced fluids were sampled at five producing wells (Fig. 1) distributed around the injection well and comprised predominantly brine with a subsidiary fractions of oil and variable proportions of CO_2. All the wells show marked increases in alkalinity during the six months after injection started in wells 37, 38 and 40. Some of this increase can be explained by dissolution of calcite in the reservoir but modelling the changes in cation concentrations and Sr-isotopic ratios requires significant dissolution of plagioclase, biotite and chlorite with potential subsequent precipitation of carbonate minerals. The observations of mineral equilibria and dissolution kinetics are compared to predictions based on laboratory experimental determinations of reaction kinetics.

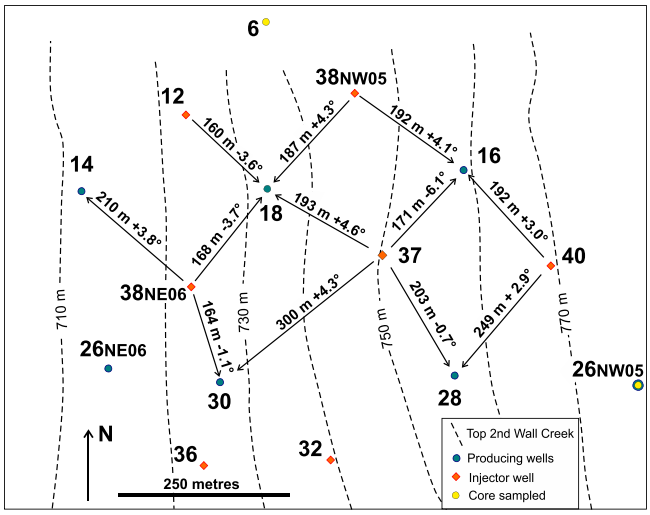


Fig. 1. Distribution of injector well, producer wells and cored wells sampled in Salt Creek Field. Distances and average slope of Wall Creek 2 sandstone given from injector wells. Contours denote depth to top of Wall Creek 2 member. Note that CO_2 injection in this field is progressing from north to south with CO_2 injection initiating in wells 12WC2NE06 and 38WC2NW05 in July 2009 with wells 14, 16 & 18 producing significant CO_2 by the start of injection in wells 38WC2NE06, 37 and 40 in September 2010. CO_2 injection commenced in wells 36 and 32 in January 2011. Core samples were taken from wells 6WC2NW05 and 26WC2NW05. Wells 12, 14, 26NE06, 36 and 38NE06, have full suffixes WC2NE06. Wells 16, 18, 26NW05, 28, 30, 32, 37, 38NW05 and 40 have full suffixes WC2NW05.

2. Field experiment: the Salt Creek Field, Wyoming

The Salt Creek Oil Field in Wyoming is contained in a ~12 km long NNW elongate domal anticline with shallowly dipping limbs. Oil was first recovered by drilling in 1908 and from the deeper 2nd Wall Creek sandstone studied here, in 1917. From 1964 oil was recovered by water flooding and in 2004 CO_2 injection for enhanced oil recovery from the 2nd Wall Creek sandstone commenced in the north of the anticline with injection progressively moving to the south.

2.1. Geological setting

The 2nd Wall Creek Sandstone at Salt Creek correlates with sandstone unit III of the upper part of the Belle Fourche Member of the Frontier Formation (Merewether et al., 1979) (the Second Frontier allomember of Bhattacharya and Willis, 2001) in eastern Wyoming. The Frontier Formation was deposited between 98 and 94 Ma (May et al., 2013). Its sedimentary structure is currently interpreted as top-truncated deltas which formed along the western margin of the Western interior seaway (e.g. Bhattacharya and Willis, 2001; Lee et al., 2005, 2007). It comprises arkoses and feldspathic litharenites with abundant volcanic rock fragments, indicating primary deposition of relatively immature sediments (Dutton et al., 2000). The 2nd Wall Creek member at Salt Creek is about 20 m thick and includes mudstone, siltstone, and sandy mudstone, planar to cross-stratified sandstones and pebble-bearing muddy-sands, sandy-muds, and mudstones. The coarsening-up sandstone units are interpreted as delta lobes with characteristic horizontal dimensions of ~1000 m (Lee et al., 2005). Diagenetic iron-bearing calcite cement occurs as nodules and larger, 25 m^2, tabular concretions following and cross-cutting bedding and occluding porosity in the coarser sandstones where carbonate contents may exceed 30% (e.g. Dutton et al., 2002).

Two cores from hole 6WC2NW05 and 26WC2NW05 through the Wall Creek 2 member within 500 m of the injection well contain sandstones comprising predominantly quartz, plagioclase (An 3 to 40%, average ~An 20%) and lithic andesitic and mudstone clasts with minor K-feldspar, chlorite, biotite and clay minerals as well as variable

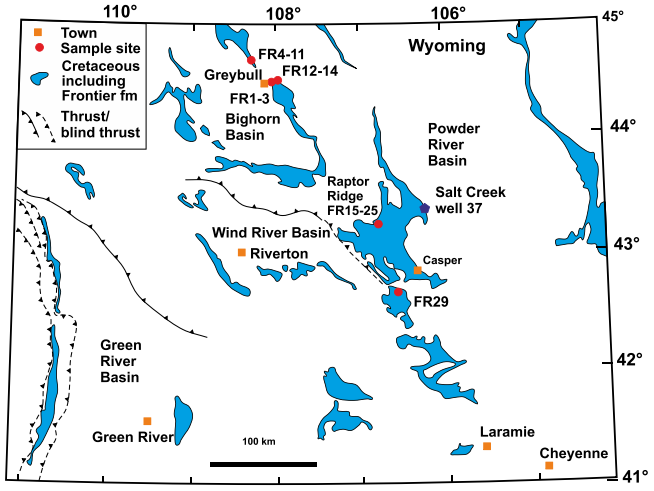


Fig. 2. Map of Wyoming showing outcrops of the Cretaceous that contain the Frontier Formation, sample sites and the location of the Salt Creek Oil Field.
Redrawn from Roberts (1989).

fractions of calcite cement (analyses of plagioclase, K-feldspar and biotites in Table S1).

The samples of the reservoir Frontier Formation have been supplemented by surface samples collected from outcrops distributed through Wyoming (Fig. 2). These sandstones are petrographically similar to the lithic arkoses from the Frewens sandstones described by Dutton et al. (2000) of which the detrital grains comprise approximately 40% quartz, 27% rock fragments (chert, volcanic, plutonic and metamorphic fragments) and about 15% plagioclase and 15% K-feldspar, with partly altered biotite and subsidiary chlorite and clay minerals. The sandstones contain abundant Fe-bearing calcite cements often present as concretions up to several metres in diameter and ~1 m thick (Dutton et al., 2002). The sampled localities represent several stratigraphic levels within the Frontier Formation. The Raptor Ridge locality (Fig. 2) is part of the Wall Creek Sandstone Member (Lee et al., 2007) which overlies the Belle Fourche Member containing the 2nd Frontier Member, the stratigraphic equivalent of the 2nd Wall Creek Sandstone at the Salt Creek field (Bhattacharya and Willis, 2001; Merewether et al., 1979). The samples from Greybull are from the Torchwood Sandstone Member thought to correlate with the 2nd Frontier member and the 2nd Wall Creek Sandstone at Salt Creek (Merewether et al., 1979).

2.2. Petrophysics

Porosity measurements calculated from gamma ray density logs are available for the injection and production wells 18, 28, 30 & 37WC2NW05 (http://wogcc.state.wy.us/). Permeabilities have been estimated by fitting a power law function to the porosity-permeability relationship measured on the nearby 1st and 2nd Wall Creek sandstone members in wells 14–10 and 12–83, the nearest comparable unit (Fig. 3). The calculated permeability distributions of the four wells with porosity measurements are shown in Fig. 4. The permeability distributions are characteristically heterogeneous with the highest permeability layer at 7 to 10 m depth, a subsidiary maximum between 12 and 17 m depth (except in well 37) and a number of subsidiary peaks. The resolution of the permeability distribution is limited by the resolution of the gamma ray density log from which the porosities were calculated which was ~35 cm. It is very probable that permeabilities exhibit larger magnitude heterogeneities on smaller scales.

The marked permeability heterogeneities will dominate the flow paths taken by the injected CO_2, the consequent flows of brine, CO_2 dissolution in brine and thus the sampling of brine and CO_2 by the production wells (Fig. 5). The order-of-magnitude lower viscosity of

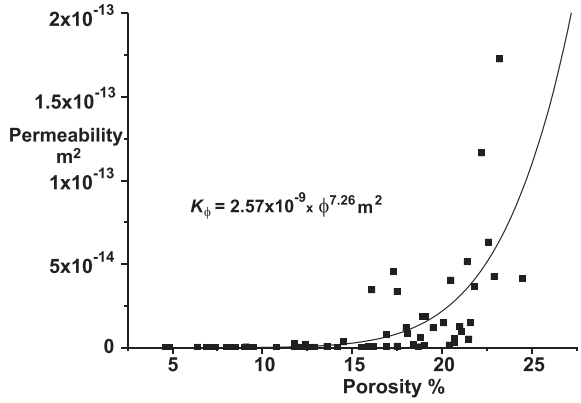


Fig. 3. Permeability-porosity relationship from measurements on core in wells 14–10 and 12–83 from the 1st and 2nd Wall Creek 1 sandstone and best fit power law curve.

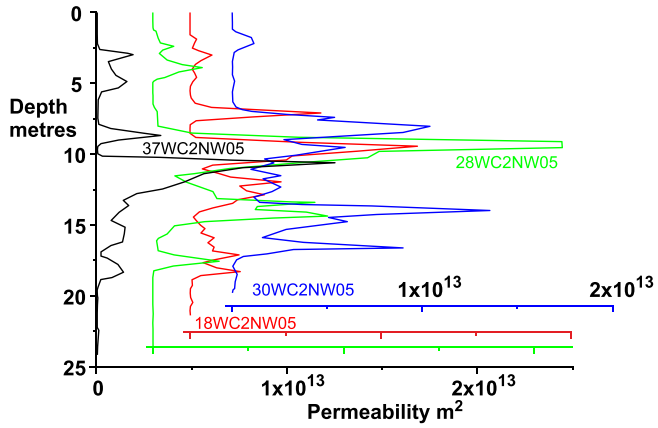


Fig. 4. Permeabilities for the four wells with gamma ray density logs calculated from fit to permeability-porosity data in Fig. 3. Note staggered *x*-axis. Depth from local top of 2nd Wall Creek sandstone.

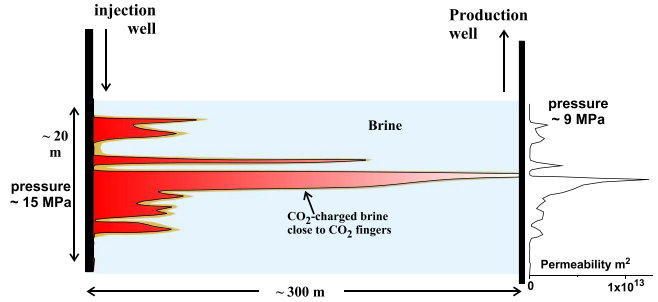


Fig. 5. Diagrammatic 2-dimensional section illustrating how CO_2 will penetrate highest permeability layers. Note expected narrow fringe to CO_2 fingers in which CO_2 diffuses into brine but flow rates in the fringe zone will be proportional to their permeability which is markedly higher than more distal brines.

supercritical CO_2 compared to water will cause CO_2 'fingers' occupying the highest permeability horizons to accelerate with time accentuating the fingering. Brine will be preferentially sampled from the 'next' highest permeability layers adjacent to the CO_2 fingers.

2.3. CO_2 injection and fluid sampling

CO_2 injection at the Salt Creek Oil field commenced in 2004 and has been progressively moved to more southerly wells. Injection is based on a five-spot model with four production wells surrounding each injection well repeating to form a continuous grid of production wells (Fig. 1).

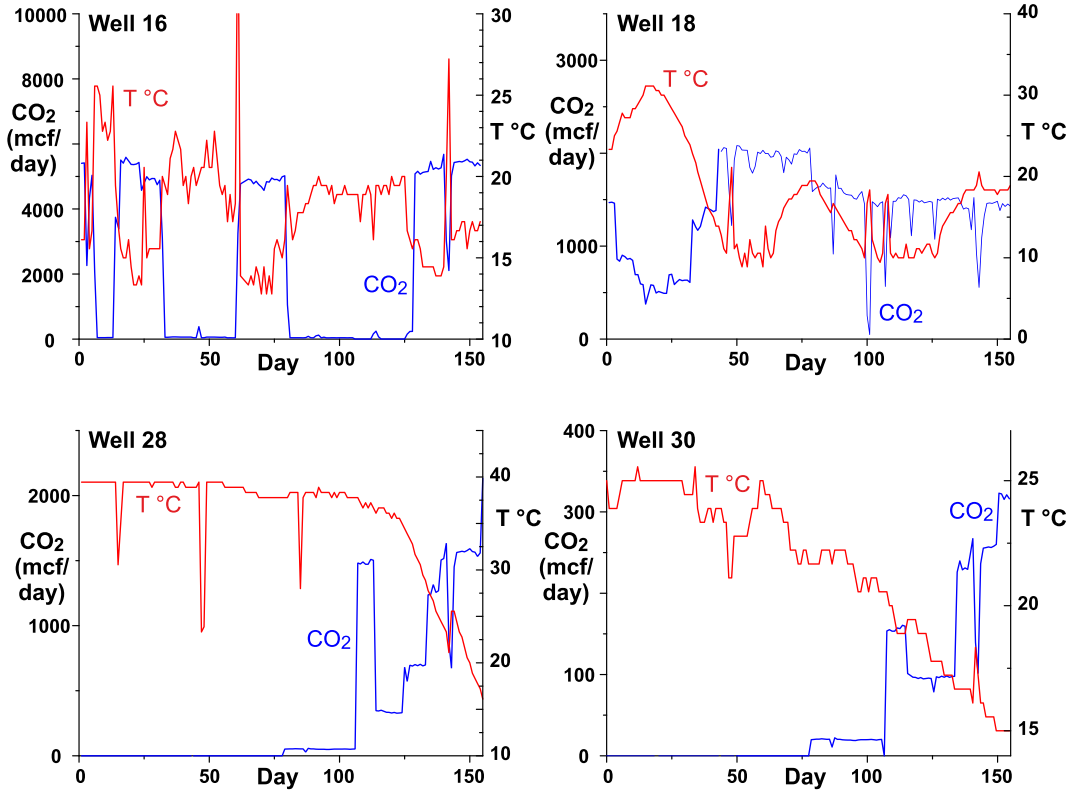


Fig. 6. Recorded CO_2 production (mcf/day) and production temperatures for wells 16, 18, 28 and 30WC2NW05. Drops in temperature reflect cooling from expansion of an increased fraction of the produced CO_2. Times of near-zero CO_2 production in well 16 reflect well shut-in.

Seismic reflection profiles were shot every month over 12 months following an early phase of CO_2 injection to the north-east of the anticline. These imaged ellipsoidal CO_2 accumulations spreading away from the injectors elongate in the up-dip direction which started merging after about 9 months (O'Brien et al., 2010).

The CO_2 injection in well 37WC2NW05, the site of this study, commenced on 14 September 2010. CO_2 injection in adjacent wells 38WC2NE06 and 40WC2NW05 started 3rd September 2010. CO_2 injection had been taking place from July 2009 through the injectors 12WC2NE06 and 38WC2NW05 north of wells 14WC2NE06, 16 and 18WC2NW05 which were already producing CO_2 by September 2010 (Fig. 6). To the south of wells 28 and 30, CO_2 injection commenced in January 2011 in wells 32WC2NW05 and 36WC2NE06. ^{3}He and ^{129}Xe noble gas isotopic spikes were added to the gas stream from 14 September 2010 during the first week of CO_2 injection in well 37 and corresponding isotopic anomalies were recorded in well 18 $<$ 8 days and in well 28 (south of the injector) ~11 days after injection commenced (Zhou et al., 2011). Some high permeability connections must be present between the injector and these wells but these would have limited vertical extents below the resolution of the porosity measurements. Significant CO_2 breakthrough in wells 28 and 30, as monitored by recorded CO_2 production at the well heads, did not occur until about 80 days after initial injection of CO_2 in well 37 although the change in well temperature of the produced fluids indicates progressive cooling from about day 40 (Fig. 6). Gas samples from Well 30 did not contain a resolvable ^{3}He spike and it is probable that the CO_2 and brine arriving at this well was dominated by the nearer injector 38WC2NE06 (Fig. 1).

The 2nd Wall Creek sandstone is at a relatively shallow depth of ~700 m and injection and extraction pressures are maintained to keep the CO_2 supercritical with a downhole injection pressure in well 37 of between 14.5 and 15.9 MPa except between days 82 and 101 after injection commenced when the CO_2 injection was paused and water injected. Downhole pressures in the production wells were maintained at between ~8.3 to 10 MPa.

Fluid samples were taken from taps off the production pipe lines where they were accessible in pump stations situated within a few hundred metres of well heads. The fluids were collected in collapsible 4L LDPE carboys fitted with polypropylene spigots at their base. The carboys were left overnight for the oil to float (fluids contained between ~0.5 and 5% oil) and the water samples taken from the spigot (c.f. Lico et al., 1982). The water was filtered through 0.2 μm nylon filters in a hand pressured tower into two 60 ml HDPE bottles, one of which was acidified with ultrapure HNO_3 to pH ~ 2. Alkalinity was determined by Gran titration on a filtered aliquot between 2 and 15 h after collection. Alkalinities measured on two unfiltered samples were similar to measurements on the filtered samples. No carbonate precipitates were observed in the carboys or on the filters. The active CO_2 degassing of the fluids precluded consistent determination of pH. Fluids were sampled daily between days 1 to 78 and days 143 to 153 after injection commenced in well 37.

2.4. Analytical methods

The element and isotopic composition of fluids sampled from the wells are presented in Supplementary material (Table S2). Major (Na, K, Ca, Mg) and minor elements (Al, Fe, Mn, Si, Sr, S) were measured on the acidified samples by Varian Vista-PRO simultaneous inductively coupled plasma-atomic emission spectrometry (ICP-AES) at the University of Cambridge following the method given in de Villiers et al. (2002) using a mixed standard with cation proportions specifically designed to match the waters. Analyses were performed against international water standards T-167, T-143, SPS-SW2 and ION-20 which reproduce to better than 6% (2σ). Fluid anion (Br, F, Cl and SO_4) composition was measured on unacidified samples using a Dionex ICS-3000 Ion Chromatography system at the University of Cambridge. Analyses were performed against international water standards T-167, T-143, P35 and

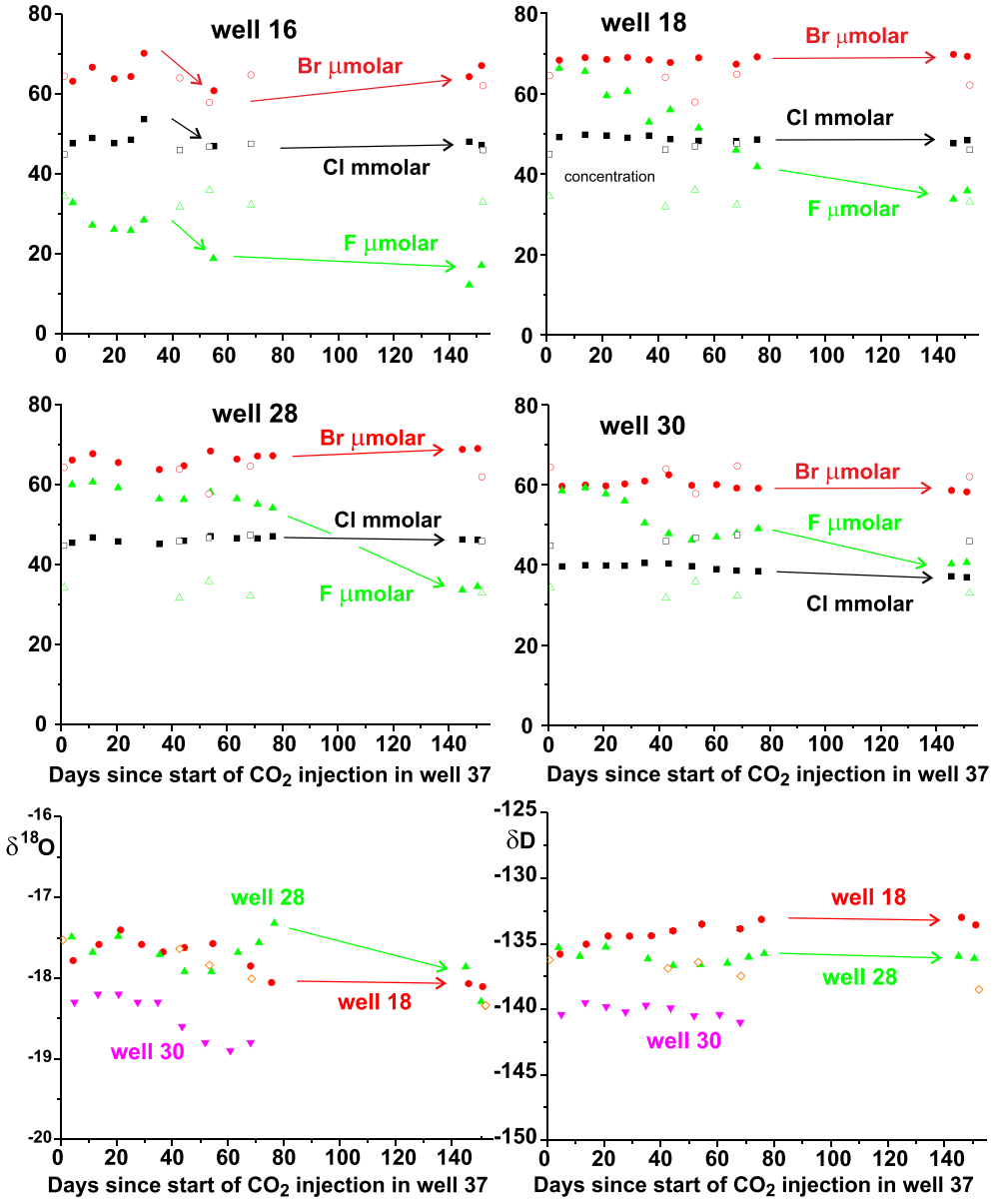


Fig. 7. Variation of anions Cl, Br, F, $\delta^{18}O$ and δD with time in sampled waters. Open symbols are analyses on injection fluids. Note that Cl and Br change very little except in well 16 just before the well was shut in from day 36. Fluorine shows a large decrease in wells 18, 28 and 30 and is low in well 16. It seems likely that SiF4 dissolves in supercritical CO_2. Data averaged over 4 to 8 day periods.

LGC6019 which reproduce to better than < 2% (2σ) for all elements analysed. $\delta^{18}O$ and δD isotopic ratios of fluids were analysed in the Godwin Labs, University of Cambridge, relative to internal standards and are expressed in ‰ deviation relative to the VSMOW standard with analytical precisions (2σ) estimated at ± 0.1 and ± 0.5‰ respectively.

Mineral compositions in core and rock samples were analysed by a Cameca SX100 electron microprobe at the Dept. Earth Sciences, University of Cambridge using 5 wavelength dispersive spectrometers and a defocused (5 μm) beam for feldspars, carbonates and biotite. 20 s counting times were used for major elements and 30 s for minor elements. Analyses were run at 15 keV with a 10 nA for all elements except Mn in carbonate (40 nA) and Ti in micas (100 nA).

Sr-isotopic ratios were determined on aliquots of the acidified fluid samples and whole rock, leaches and mineral separates of core samples at the University of Cambridge following Bickle et al. (2003). The standard NBS 987 gave 0.710259 ± 0.000009 (1σ) on 70 separate measurements made during the course of these analyses. Strontium blanks were always negligible compared to the Sr concentration of these samples. Core, mineral and two rock samples were leached to determine the Sr-isotopic composition of carbonate and silicate mineral fractions (methods in Table S3, supplementary information). The leaching procedure followed that of Bickle et al. (2015) with the finely ground rock powder first washed in water to remove loosely held Sr, followed by leaching in cold 10% acetic acid overnight to dissolve carbonate, then leached cold in 1 M HCl to remove any residual carbonate. Samples were rinsed in water between the leaching steps. The silicate residue from the leaching steps was ignited at > 900 °C to remove organics and taken into solution using HF + HNO_3, HNO_3 and then HCl in Teflon lined pressure vessels at 180 °C (full details in Table S3, supplementary materials). Concentrations of the elements (Na, K, Ca, Mg, Al, Fe, Mn, Sr, S) were analysed on aliquots of the leachates and residue by ICP-AES using the same methods as for the waters but with synthetic standards matching the sample concentrations and checked against analysis of a complete digestion of USGS rock standard SCO-1. Sums of the leachate and residue elemental compositions were compared to analyses of the bulk powder and gave total concentrations on four samples which averaged only 9% less than the corresponding whole rock compositions (Table S3). Samples A2392 and B11/2/2438 gave large ~100% discrepancies and the whole rock compositions seem low in many elements for these cores. Si concentrations in analyses of

residues and whole rocks are calculated by difference as these samples were dissolved by HF dissolutions. Lithic fragments, volcanic clasts and detrital plagioclase were handpicked from the core sample A2334. Their cation concentrations indicate that all these fractions contained significant calcite and the plagioclase is partly altered to clay minerals.

Thermodynamic calculations of fluid compositions at various CO_2 and mineral saturations are carried out using PHREEQC 3.3.8.11728 with the PHREEQC and LnLL databases (Parkhurst and Appelo, 2013).

3. Fluid geochemical evolution at Salt Creek

The evolution of the sampled fluid chemistry is expected to reflect progressive fluid-mineral reactions buffering the increase in acidity as the CO_2 content increases. Interpretation of the changes in fluid chemistry is potentially complicated by the previous history of oil extraction and water injection in the oil field.

The aqueous formation fluids in the 2nd Wall Creek sandstone are dilute brines. Analyses of the formation fluids from across the field sampled in early 1920s (Young and Estabrook, 1925; Estabrook, 1925) and given in oil field reports in 1979, 1987 and 1996 have Na between 170 and 290, Ca 0.3 to 0.7, and Cl between 80 and 205 mmol/kg with Na/Cl molar ratios between 1.2 and 1.8. Analyses of waters collected from the 2nd Wall Creek sandstone in Teapot Dome, 20 km south-east of the Salt Creek field, in 2009 have more dilute compositions (Na 65 and 90, Ca 0.24 and 0.33 and Cl 34 and 46 mmol/kg, Table S4) but this field has also been subject to a range of oil recovery techniques. The most dilute fluids sampled in this study, the initial fluids sampled in wells 28 and 30, have similarly more dilute Cl and Na concentrations of ~45 and ~80 mmol/kg, but higher Ca at ~1.6 and 2.9 mmol/kg. The northerly wells, which were being fed CO_2 from injectors to the north, had similar Cl (43 to 49 mmol/kg) but higher Na and Ca at ~105 and 3.7 to 5.4 mmol/kg.

The Salt Creek field has been subject to extensive water flooding with water obtained from the deeper Madison and Tensleep Formations. These have Na ~ 30, Ca ~ 7 to 10 and Cl 16 to 26 mmol/kg (Oil well reports, Table S4). The waters currently being injected comprise a mixture of all the produced waters after separation of CO_2 and oil. These were sampled intermittently during the injection period and have compositions intermediate between the initial dilute fluids sampled in wells 28 and 30 and the wells with more concentrated cations (wells 16 and 18) (Figs. 7–9).

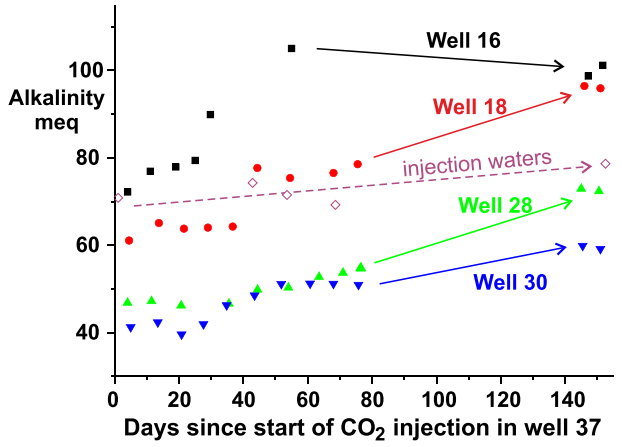


Fig. 8. Variation in alkalinity in produced waters over period after CO_2 injection commenced in well 37. Note that wells to the north already producing significant CO_2 have high initial alkalinities but these continue to rise. Wells 28 and 30 to the south of well 37 have low initial alkalinities which rise progressively during the sampling period. Data averaged over 4 to 8 day periods.

3.1. Sources of fluids: conservative tracers and alkalinities

The initial fluids present in the 2nd Wall Creek sandstone at the start of CO_2 injection reflect the complex prior history of the oil field. A key question is the extent to which the systematic changes in alkalinity and concentrations of Ca, Na and other cations (Figs. 8 & 9) after CO_2 injection commenced, are the result of fluid-mineral reactions or reflect changes in water composition, particularly penetration of the injected waters. The concentrations of the conservative tracers, Cl and Br, change little over the injection period (Fig. 7). Well 16 produced significant CO_2 relatively early in our experiment and both Cl and Br show a rapid increase as the well approached saturation by CO_2, possibly as the residual brine was dehydrated by the CO_2. F drops markedly associated with increases in produced CO_2 (wells 18, 28 and 30), possibly because SiF_4 is soluble in supercritical CO_2. The stable isotope ratios of oxygen and hydrogen exhibit small changes with time (Fig. 7) presumably reflecting fluid heterogeneity within the formations.

The consistency of Cl at ~45 to 50 mmol/kg in wells 14, 16, 18 and 28 as well as in the injected brines and only marginally less at ~40 mmol/kg in well 30, compared with the much higher historical concentrations of ~150 mmol/kg, suggests that the accessible parts of the reservoir have been completely flushed during the water flooding leaving the 2nd Wall Creek sandstone with relatively uniform fluid compositions. In contrast the cations show marked changes related to CO_2 injection.

Alkalinity rises markedly in all the wells (Fig. 8). Wells 16 and 18 to the north already producing significant CO_2 have initial alkalinities and water cation concentrations similar to the injected waters but these concentrations continue to rise. Wells 28 and 30 to the south of well 37 have low initial alkalinities which rise progressively during the sampling period. In all the wells the rise in alkalinity is supported by a corresponding rise in Na, Ca, Mg, K and Sr. Since Cl changes little, the increase in Na which contributes between ~50 to 75% of the rise in alkalinity, cannot be attributed to mixing with more saline brines.

The difference between the element ratios of the injected waters and element ratios of the cations added to the produced waters, calculated by taking the difference between the waters sampled over the last 11 days and those sampled over the first 20 days (Fig. 10), shows that the changes in water composition are not explained by increases in the fraction of injection water. Note that injection waters likely to be sampled are those injected prior to the sampling for this project whereas those we analysed were collected during the course of this project. The small rise of injected water cation concentrations during the sample period suggests that concentrations in the older injected waters were correspondingly slightly lower.

This conclusion, that changes in the background brine compositions had a limited impact on the composition of the produced fluids, is supported by the changes of Sr-isotopic ratios in the produced fluids (Fig. 9). The injection fluids have $^{87}Sr/^{86}Sr$ ratios between 0.71078 and 0.71092, less than well 18 (0.71305 to 0.71394), 28 (0.71137 to 0.71168) and well 30 (0.71309 to 0.71382). Only fluids from well 16 (0.710336 to 0.71137) scatter about the composition of the injection fluids. The fluid Sr concentrations in wells 18, 28 and 30 increase by between 66 and 100% over the sampling period. Fig. 11 shows the expected trajectories of the initial waters as fluid with the composition of the injection waters is mixed with the initial waters sampled in each well. It is clear that the Sr-isotopic evolution of the wells is dominated by addition of Sr from a source distinct from that of the injection fluids, presumably from dissolution of minerals.

3.2. Sources of fluids: modelling inputs of injection fluids and fluid-mineral reactions

The changes of water compositions resulting from addition of injection waters and dissolution or precipitation of minerals may be modelled by mass balance of the stoichiometric cations (c.f. Kampman

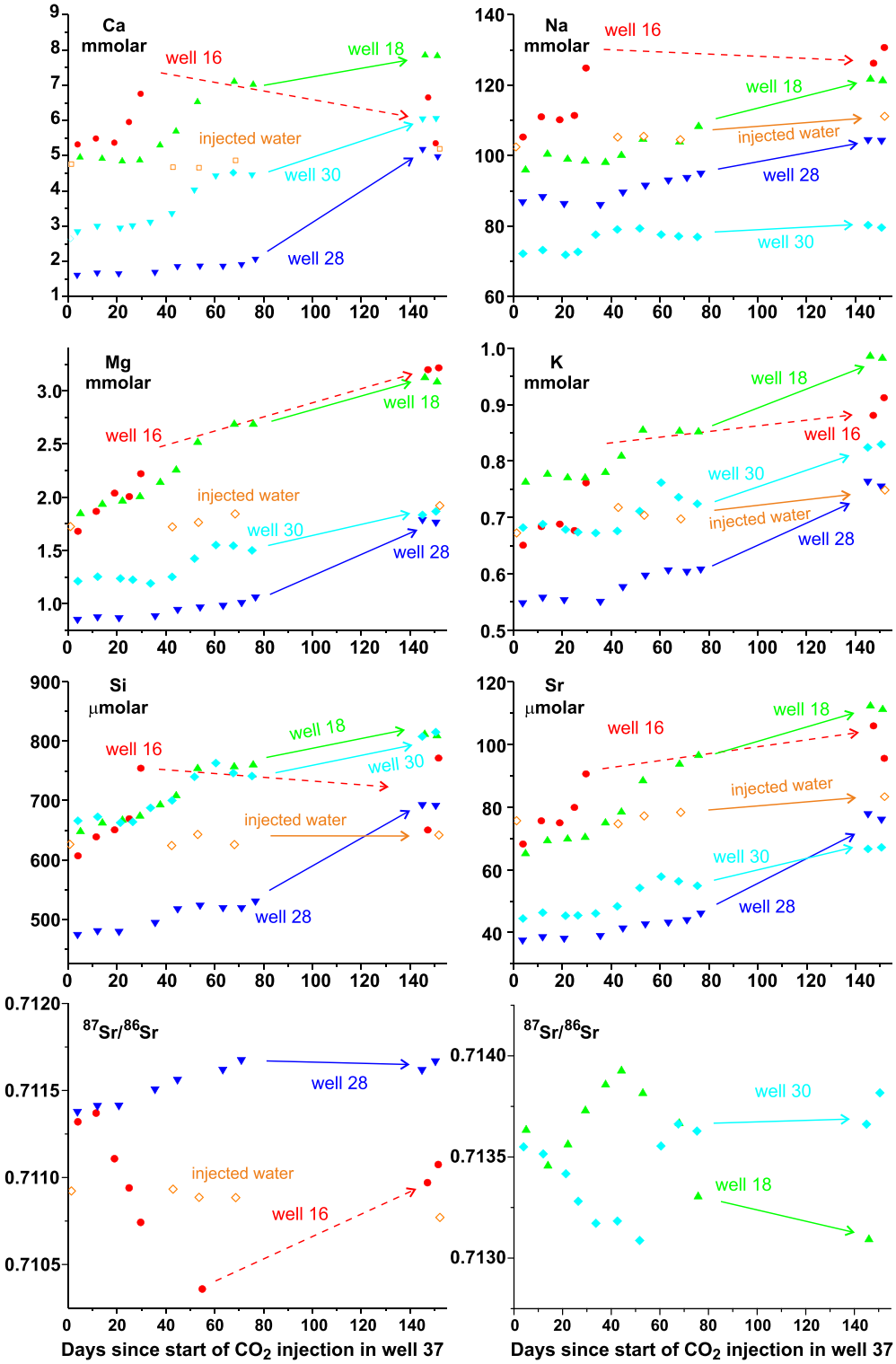


Fig. 9. Variation in Ca, Na, Mg, K, Si, Sr and $^{87}Sr/^{86}Sr$ ratios in produced waters with time after commencement of CO_2 injection in well 37. Data averaged over 4 to 8 day periods. Open symbols are of injection waters.

et al., 2009). The mass balance equation may be written

$$C_i^f - C_i^I = \sum_{j=1}^{n} X_j \alpha_i^j \quad (1)$$

where C_i^f is the final fluid concentration and C_i^I is the initial fluid concentration of component, i (mmol/kg). α_i^j is the concentration of component i in mineral phase j (mole fraction) and X_j is the mass (mmols) of phase j added to (positive), or precipitated from (negative), the fluid. Eq. (1) is solved for the n unknowns X_j by the routines in Kent et al. (1990) with the uncertainties on C_i^f, C_i^I, and α_i^j propagated through the calculation. The uncertainties on the initial and final fluid compositions are taken as the standard error on the average of the first 5 fluid samples ($\sigma/\sqrt{5}$), and last 5 fluid samples analysed. The uncertainty on the mineral compositions is taken as the standard error on the mineral microprobe analyses for calcite, plagioclase and biotite (Table 1), as 5% of the concentration for the elemental compositions of

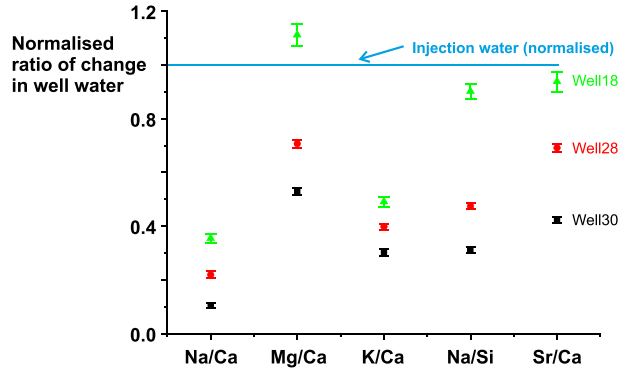


Fig. 10. Molar element ratios of the cations added to the produced waters normalised to the element ratios in the injected waters. The concentration of cations added to waters from each well over the sampling period was calculated by taking the difference between the waters sampled over the last 11 days and those sampled over the first 20 days and the 1σ error bars calculated from the standard errors (where n is the number samples) on the set of samples averaged.

chlorite and smectite and 0.5% of the components in kaolinite. Solutions are illustrated in Fig. 12.

The results imply that the chemical evolution of the fluids is dominated by the dissolution of plagioclase, chlorite and biotite and calcite except in Well 16 where calcite modes are within error of zero. Smectite precipitates. The kaolinite mode is within error of zero.

It should be noted that fluids sampled will be mixtures that range from CO_2-saturated fluids flowing close to the CO_2 penetrating high permeability layers to fluids far from CO_2 fingers that are little changed in composition. Since CO_2 will penetrate the highest permeability layers, the brines flowing adjacent to the CO_2 occupying the next most permeable layers will be preferentially sampled in the produced waters. Thermodynamic modelling of fluid-mineral reactions suggests that CO_2-saturated fluids will initially dissolve calcite but re-precipitate carbonates at later times as silicate dissolution raises fluid alkalinity (e.g. Xu et al., 2007; Dubacq et al., 2012). The decrease in calcite dissolution mode from the least evolved fluids from Well 30 to the most evolved from Well 16 is consistent with this prediction and implies that the more reacted CO_2-saturated fluids are precipitating calcite.

3.3. Sr and Sr-isotopic systematics

Sr and $^{87}Sr/^{86}Sr$ ratios put constraints on the fluid and mineral interactions. The Sr-isotopic ratios and Sr and major cation concentrations have been determined on whole-rock samples, carbonate leaches and silicate residues and some hand-picked feldspars, lithic and volcanic clasts from drill core through the Frontier formation in the Salt Creek field and from outcrops of the Frontier Formation in Wyoming (Figs. 1 & 2, Supplementary data Table S3, Fig. 13). The Sr-isotopic compositions of the carbonate leaches and the carbonate-cemented high CaO whole rock samples imply carbonate $^{87}Sr/^{86}Sr$ ratios of between 0.7075 and 0.7078 which are only marginally higher than seawater $^{87}Sr/^{86}Sr$ ratios of ~0.7074 at the time the Frontier Formation was deposited. The low-Ca silicate-dominated samples exhibit a wide scatter of $^{87}Sr/^{86}Sr$ ratios of between 0.706 and 0.720 which reflects the heterogeneous source terrain for the Frontier Formation which comprised contemporary Cordilleran magmatic arc igneous rocks and older Proterozoic and Archaean basement (e.g. May et al., 2013).

The carbonate leaches, silicate residues from leaching, the whole core samples and the lithic and volcanic clasts from core samples from holes 6WC2NW05 and 26WC2NW05 drilled in 1972 at Salt Creek all have low $^{87}Sr/^{86}Sr$ ratios (0.706 to 0.7088, Table S3) reflecting the dominance of Cordilleran igneous material in this sediment. Only the feldspar fraction has a slightly higher $^{87}Sr/^{86}Sr$ ratio of ~0.7106. However, from the significantly higher $^{87}Sr/^{86}Sr$ ratios of the initial formation fluids (Figs. 9 & 11) and the approximately constant or increase in $^{87}Sr/^{86}Sr$ ratios in wells 18, 28 and 30 during the sampling period, we infer that the Sr-isotopic compositions of the silicate material in the Frontier Formation at Salt Creek exhibits a similar distribution to samples collected from surface outcrops (Fig. 13).

Calculation of the change in fluid $^{87}Sr/^{86}Sr$ ratios provides a test of the consistency between the calculations of the mineral modes consumed and precipitated over the sampling period. The change in cumulate mineral inputs or outputs, calculated as in Section 3.2 above,

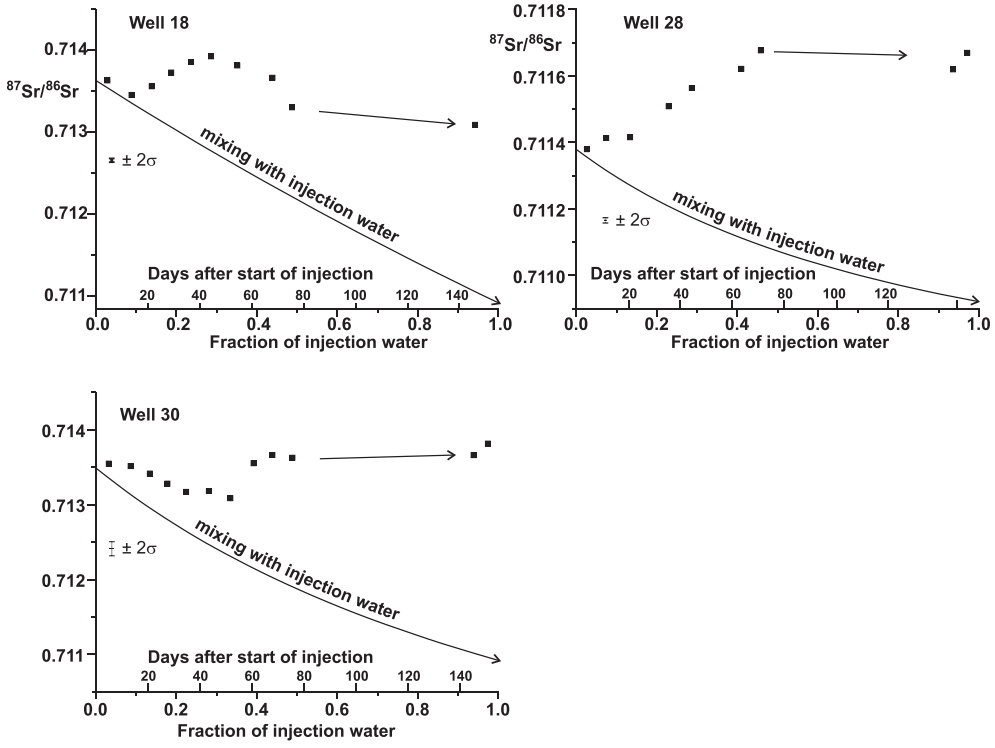


Fig. 11. Calculated mixing curves for $^{87}Sr/^{86}Sr$ ratios between initial fluid samples from wells 18, 28 and 30 as a function of the fraction of initial water added (values below *x*-axis) compared with time evolution of the sampled fluids (days since injection started given above *x*-axis).

Table 1
Compositions of minerals used in mass balance calculations.

	Calcite[a]	1σ	Plagioclase[a]	1σ	Chlorite[b]	1σ	Biotite[a]	1σ	Kaolinite[c]	1σ	Smectite[b]	1σ
SiO_2			2.776	0.014	2.688	0.027	2.801	0.024	2.00	0.01	3.55	0.04
$Al(O_{1.5})$			1.224	0.014	3.050	0.031	1.419	0.036	2.00	0.02	1.88	0.02
FeO	0.014	0.001	0.007	0.001	1.300	0.065	1.373	0.063			0.35	0.02
MgO	0.006	0.003	0.001	0.000	2.010	0.101	1.109	0.040			0.37	0.02
CaO	0.967	0.006	0.217	0.015			0.015	0.002			0.20	0.01
$Na(O_{0.5})$			0.755	0.016			0.050	0.003			0.09	0.00
$K(O_{0.5})$			0.039	0.003			0.733	0.025			0.23	0.01
Sr(1000)	1.420	0.100	3.00[d]	0.41	0.006		0.047[e]		0.15[e]		0.23[e]	
$^{87}Sr/^{86}Sr$	0.7076											

[a] Average compositions of minerals used in mass balance calculations taken from Table S1 in supplementary information.
[b] Average chlorite and average continental smectite from Bickle et al. (2015).
[c] Ideal composition.
[d] Estimated from residues from leaching Frontier Formation sandstones.
[e] Biotite and clay mineral Sr concentrations taken from Garçon et al. (2014).

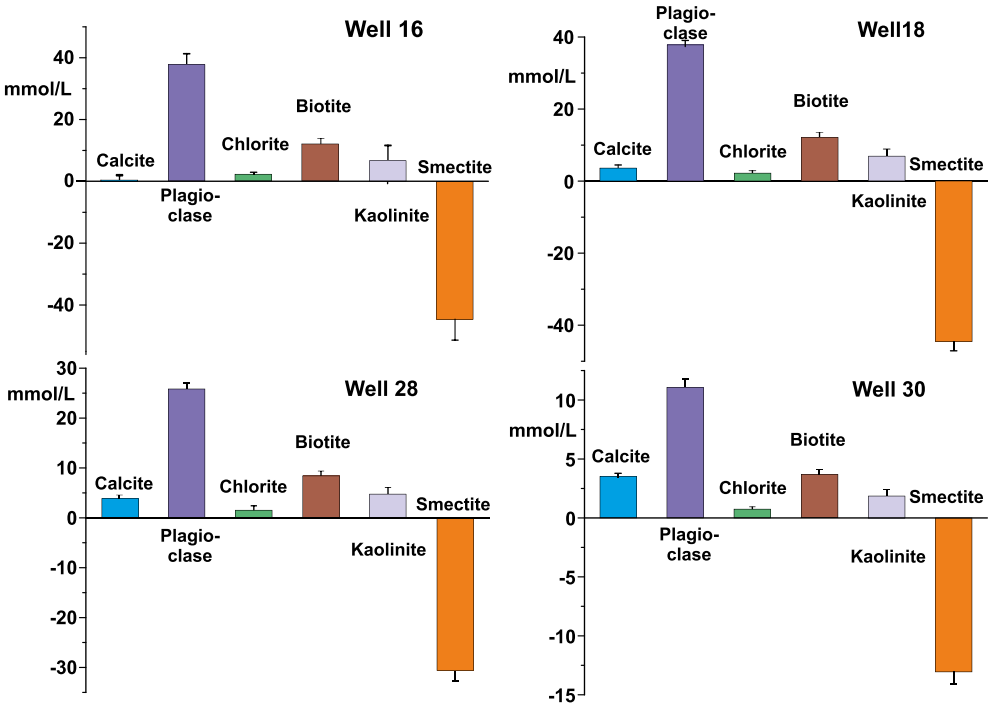


Fig. 12. Mineral inputs (negative for precipitation) in mmol/L calculated from difference between initial and final fluid samples (Eq. (1)) for the four wells and solved for the components Si-Al-Mg-Ca-Na-K. Error bars are 1σ calculated from uncertainties in mineral and fluid compositions.

from the difference in chemistry between the initial sampling period and the given sampling period, is illustrated in Fig. 14. Precipitation of primary silicates plagioclase or biotite implied by decreasing mode with time coupled with dissolution of smectites as exhibited by Well 30 between days 50 to 75 is most likely explained by mixing of waters with different extents of fluid-mineral reactions. Significant low temperature precipitation of plagioclase or biotite or dissolution of smectites is thought improbable.

The mineral modes may be used to predict the changes in fluid Sr concentrations and $^{87}Sr/^{86}Sr$ ratios if their Sr contents and $^{87}Sr/^{86}Sr$ ratios are known. The Sr content of the carbonate is constrained by the acetic acid leaches of the outcrop samples of the Frontier Formation samples (Table S3) where the samples with > 2000 mmol/kg Ca have Sr/Ca ratios of 1.42 ± 0.10 (1 standard error). The two acetic acid leaches (Sr/Ca = 1.1 and 1.4) lie within this range. The acetic acid leaches of the core samples have rather higher Sr/Ca ratios but most of these have relatively low Ca concentrations (below 350 mmol/kg) and may have leached a minor silicate component. The $^{87}Sr/^{86}Sr$ ratio of the carbonate component is taken as 0.70755, the mean of the two carbonate leaches from samples collected at Raptor Ridge (Fig. 2). The mean of the acetic acid leaches of the core samples is only marginally lower at 0.7074.

Plagioclase probably contains the bulk of the Sr in the silicate fractions in the Wall Creek 2 sandstones. The silicate residues of the low Ca Frontier Formation sandstones and the silicate residues of the core samples have Na/Ca ratios that range between ~3 and 12 (mean 5.7) which would correspond to plagioclase anorthite contents between 8 and 23% (mean 15%). The plagioclase feldspars from the core samples (Table S1) exhibit an even wider range of compositions (An 3 to 49%, mean An 21%). It is likely that the feldspars exhibit a corresponding wide range of Sr contents. The Sr concentration of plagioclase is therefore first estimated at 3.0 mmol/mol (equivalent to ~460 ppm) from the mean Sr/Na and Na/Ca ratios of the silicate residues of the low-Ca Frontier formation outcrop samples. The other silicate minerals contain small amounts of Sr and their nominal concentrations estimated from literature values are given in Table 1.

The Sr concentration in the sampled fluids is then predicted as a function of time given the changes in cumulate mineral modes dissolved/precipitated illustrated in Fig. 15. To allow for the uncertainty in the plagioclase Sr concentration, the magnitude of the summed silicate Sr contribution was then adjusted by the factor, *f*, to give a least-squares best fit to the measured water Sr concentrations. The factor *f* is

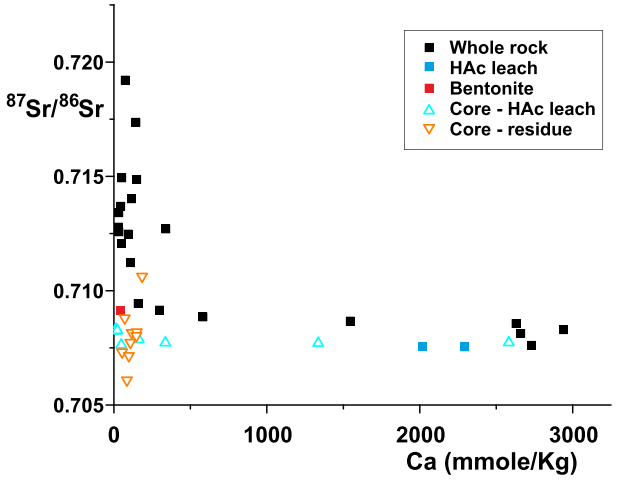


Fig. 13. $^{87}Sr/^{86}Sr$ ratios versus Ca concentration as a proxy for carbonate content for whole-rock and 2 leaches of whole-rock samples from outcrops of the Frontier Formation in Wyoming (locations on Fig. 2) and leaches and residues from leaching of core through the 2nd Wall Creek sandstone at Salt Creek (localities on Fig. 1) (see Supplementary data Table S3). The high-Ca leaches imply carbonate $^{87}Sr/^{86}Sr$ ratios of between 0.7075 and 0.7078 which are marginally higher than seawater $^{87}Sr/^{86}Sr$ ratios of ~0.7074 at the time the Frontier Formation was deposited.

then calculated by finding the value that minimises a χ^2 variable

$$\chi^2 = \sum_{i=1}^{n} \left(\frac{(Sr_C^i - Sr_M^i)}{\sigma_{Sr_M}^i} \right)^2 \quad (2)$$

where $Sr_C{}^i$ is the Sr concentration calculated from the mineral modes given their Sr concentrations in Table 1, $Sr_M{}^i$ is the measured Sr concentration and σ_{Sr_M} the estimated uncertainty of the measured Sr concentration. The results are shown in Fig. 15 and the adjustment factors vary between 0.43 and 0.62 (0.196 for the first period in well 30). This suggests that the estimate of plagioclase Sr concentration of 3 mmol/mol is high by a factor of two, well within the scatter of Sr/Na ratios. The calculations of the summed silicate Sr input are relatively insensitive to the estimate of the carbonate Sr content. For example if this is varied between 0.7 and 2.8 mmol/mol in Well 28 the factors needed to change the silicate input vary only between 0.43 and 0.34. In general the calculated time variation of the Sr concentrations matches the observed variations close to the uncertainties in the measured Sr concentrations estimated from the standard deviation of the sample sets in the time intervals. The most obvious discrepancies are between days ~25 and 75 in Well 30. Here the falls in modal plagioclase and biotite and decrease in modal smectite are interpreted to relate to mixing of less reacted fluids as decreases in plagioclase and biotite are very unlikely to result from precipitation of these minerals. The discrepancies most likely reflect heterogeneity of fluid sources and paths within the reservoir as indicated by the modelling of $^{87}Sr/^{86}Sr$ ratios.

Given the best fit Sr-concentration models, the silicate $^{87}Sr/^{86}Sr$ ratio which gave a best least-squares fit to the Sr-isotope data was calculated for each of the sampled wells (Fig. 15) by minimising a routine similar to Eq. (2) with Sr concentrations replaced by $^{87}Sr/^{86}Sr$ ratios multiplied by the Sr content. Again the best fits match the observed evolution of $^{87}Sr/^{86}Sr$ ratios well except for the period around 50 days in Well 30 and a comparable period in Well 18.The silicate $^{87}Sr/^{86}Sr$ ratios deduced from the best fits range from 0.71053 in Well 16 to 0.71429 in Well 30. These are within the range of silicate Sr-isotopic ratios analysed in the core and outcrop rock samples (0.707 to 0.719).

The calculated water Sr and $^{87}Sr/^{86}Sr$ ratios for Wells 16 and 28 match the observed changes well. The discrepancies in both Sr and $^{87}Sr/^{86}Sr$ ratios between days 30 to 75 in Well 30 have been discussed above and are best explained by arrival of waters with a different reaction history. Likewise the rather poor fit to the measured $^{87}Sr/^{86}Sr$

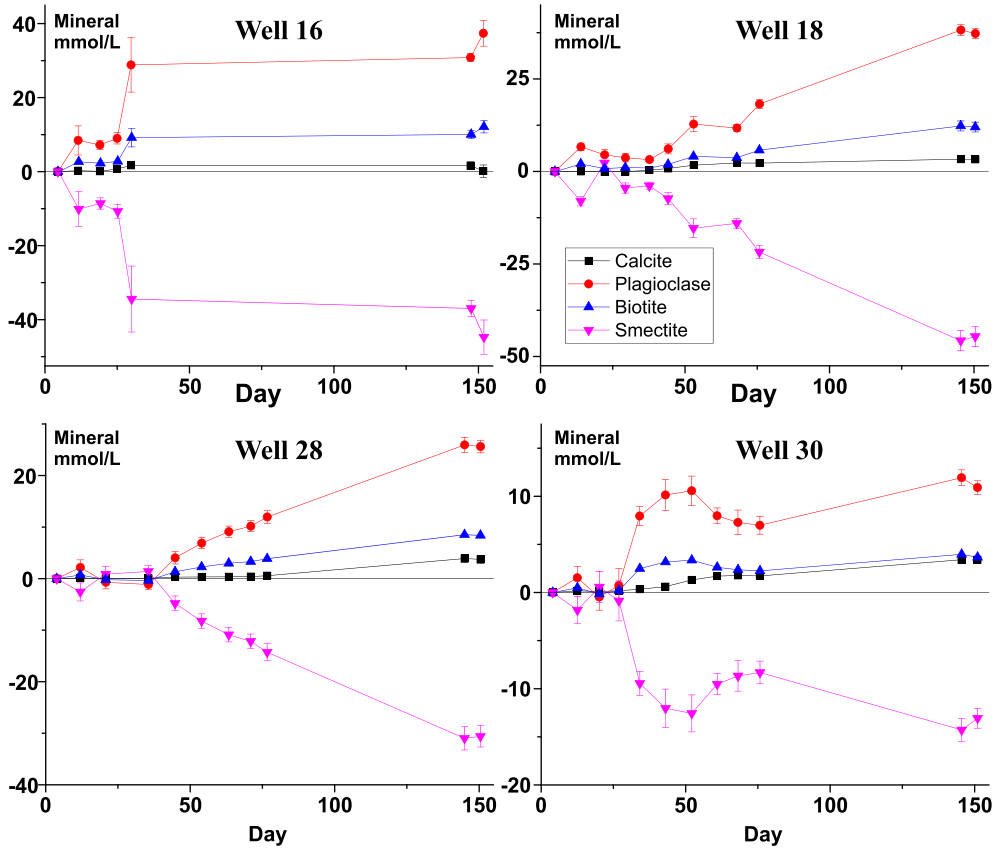


Fig. 14. Cumulative calculated mineral dissolution (+ ve) or precipitation (− ve) from sampled fluids calculated from the difference between each sampling period and the initial sampling period using Eq. (1). Error bars 1σ.

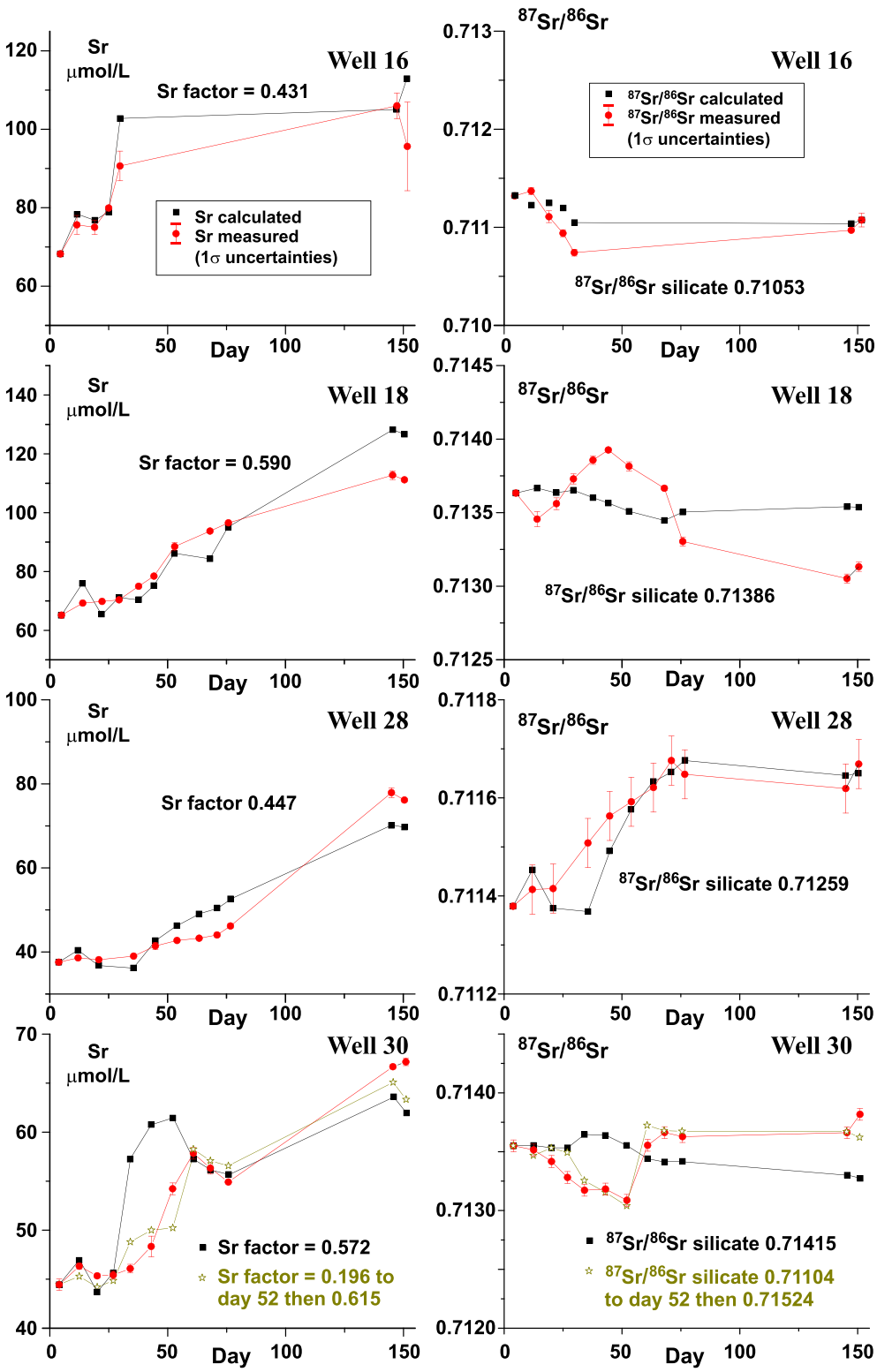


Fig. 15. Left-hand panels show measured fluid Sr concentrations (red circles, means of groups of 3 to 5 days of samples with error bars 1 standard error on mean) compared to best least-squares-fit Sr concentrations calculated from mineral modes with silicate Sr concentration adjusted by the factor given on the figure (black squares). Right-hand panels show best fit between measured (red circles) and calculated $^{87}Sr/^{86}Sr$ ratios (black squares) with silicate $^{87}Sr/^{86}Sr$ ratio adjusted to value shown. Two solutions are shown for Well 30. One (black squares) shows a profile fit with a single silicate Sr factor and silicate $^{87}Sr/^{86}Sr$ ratio and the second (stars) a fit that derived a silicate Sr factor and $^{87}Sr/^{86}Sr$ ratio for days 4 to 52, then held these parameters fixed for days 4 to 52 and minimised the misfit in Sr and $^{87}Sr/^{86}Sr$ ratio to derive best fit values of the silicate Sr factor and $^{87}Sr/^{86}Sr$ ratio for days 61 to 151. (For interpretation of the references to color in this figure legend, the reader is referred to the web version of this article.)

ratios in Well 18 may be explained by waters arriving along flow paths with differing $^{87}Sr/^{86}Sr$ ratios. The fits to Well 30's Sr and $^{87}Sr/^{86}Sr$ profiles is well matched with a change in Sr factor and silicate $^{87}Sr/^{86}Sr$ ratio at day 52 (Fig. 15). The observed scatter in $^{87}Sr/^{86}Sr$ ratios in sampled outcrop (Fig. 13) suggests that units in the deltaic 2nd Wall Creek sandstone are distinctly heterogeneous in Sr-isotopic composition. The range of the inferred silicate Sr-isotopic compositions and the apparent relative consistency of inferred isotopic compositions within the individual wells implies that the injected fluids are sampling relatively coherent beds within the deltaic 2nd Wall Creek sandstone.

The Sr-isotopic ratios confirm the results of the calculations of changes in modal mineralogy that the CO_2 injection results in significant dissolution of silicate minerals in a relatively short time period.

4. Mineral-fluid reactions and reaction rates

The fundamental process controlling the rates of fluid-mineral reactions is the rate at which CO_2 dissolves in the formation brines. In this experiment with fluids sampled at surface after they have undergone significant decompression, direct measurements of fluid CO_2 contents are not possible. Below we make thermodynamic estimates of the undegassed fluid compositions based on two approaches. 1) Calcite dissolution reaction rates are fast and it is possible to calculate the fluid partial CO_2 pressure for equilibrium with calcite. 2) The observed plagioclase dissolution implies significant fluid undersaturation which again is a function of fluid CO_2 partial pressure.

4.1. Approach to calcite-fluid equilibrium

The approach of calcite to equilibrium with the formation brines is governed by the degree of thermodynamic disequilibrium between the calcite and brine and the rate at which CO_2 is being transported by either diffusion or advection through the brine. The dissolution rate for calcite (R_T, mol·m^{-2}·s^{-1}) may be expressed as

$$R_T = K_R f(\Delta G) = K_R\left[1 - \left(\frac{\Omega}{K_{sp}^0}\right)^n\right] \tag{3}$$

where K_R is a rate constant (mol·m^{-2}·s^{-1}), which is in general a function of temperature and fluid composition and ΔG (kJ/mol) is a measure of the distance from thermodynamic equilibrium between calcite and the fluid. Transition state theory (e.g. Aagaard and Helegeson, 1982) suggests that ΔG has the form in Eq. (3) where Ω is the activity product and $K_{sp}{}^0$ is the solubility product (equilibrium constant) but this is uncertain (e.g. Hellmann and Tisserand, 2006). However in most published expressions $f(\Delta G)$ tends to a constant far from equilibrium and for calcite n ~ 1.

The rate constant, K_R, for calcite is a function of pH, temperature, CO_2 partial pressure and other components in the fluid phase. Pokrovsky et al. (2009) note that when recalculated to constant pH = 5, calcite dissolution rates exhibit a maximum at ~4 MPa and are only weakly dependent on temperature. The rates range between 1.8×10^{-5} and 3×10^{-4} mol·m^{-2}·s^{-1}.

The change in Ca concentration (Ca, mol·m^{-3}) of the fluid with time (t, s) due to surface dissolution of calcite can be written

$$\varphi\frac{\partial \mathrm{Ca}}{\partial t} = K_R\alpha\left(1 - \frac{\Omega}{K_{sp}^0}\right) \tag{4}$$

where ϕ is porosity and α is reactive surface area of calcite (m^2/m^3) in the rock. The ratio of the activity product to solubility product ($\Omega/K_{sp}{}^0$) is approximately proportional to fluid Ca content ratioed to the Ca content in equilibrium with calcite (Ca_{eq}) (Fig. 16) which allows Eq. (4) to be rewritten

$$\frac{\partial \mathrm{Ca}'}{\partial t} = K''(1 - \mathrm{Ca}') \tag{5}$$

where Ca′ = Ca/Ca_{eq} and K'' (s^{-1}) is given by

$$K'' = \frac{K_R\alpha}{\varphi\, Ca_{eq}}. \tag{6}$$

K'' = 0.087 s^{-1} for a far-from-equilibrium calcite dissolution rate of $K_R = 1.8 \times 10^{-5}$ mol·m^{-2}·s^{-1} (Pokrovsky et al., 2009), 1 vol% calcite in the rock with a surface area of ~2.5×10^4 m^2/m^3 (chosen as a minimal calcite content), porosity ϕ = 0.2 and equilibrium Ca concentration (Ca_{eq}) of 26 mol/m^3.

The dominant transport of CO_2 and Ca in the fluid may be by diffusion (e.g. close to CO_2 fingers) or by advection in the flowing brines. The differential equation describing diffusion and reaction with linear kinetics (c.f. Lichtner, 1988) is

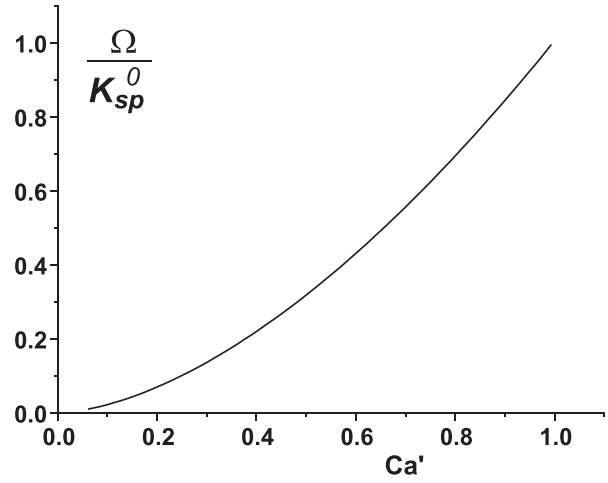


Fig. 16. Variation of calcite saturation state as a function of fluid Ca′ concentration (Ca′ = Ca/Ca_{eq}) calculated for initial fluid sample SCR-7-28 saturated in CO_2 at 10 MPa and 50 °C. Ca_{eq} = 26 mmol/L.

$$\varphi\frac{\partial \mathrm{Ca}}{\partial t} = \frac{\varphi D}{\tau}\frac{\partial^2 \mathrm{Ca}}{\partial x^2} + K_R\alpha\left(1 - \mathrm{Ca}/\mathrm{Ca}_{eq}\right) \tag{7}$$

Non-dimensionalising Eq. (7) by the transformations.

$$\mathrm{Ca} = \mathrm{Ca}'\mathrm{Ca}_{eq} \tag{8}$$

$$x = x'\, l \tag{9}$$

$$t = t'\frac{l^2}{\mathrm{D}} \tag{10}$$

where Ca_{eq} is the fluid Ca concentration in equilibrium with CO_2 saturated fluid, l is an appropriate length scale (e.g. transport distance) and D is the diffusion coefficient, gives

$$\frac{\partial Ca'}{\partial t'} = \frac{\partial^2 Ca'}{\partial x'^2} + N_D^{diff}(1 - Ca') \tag{11}$$

where, the dimensionless constant, a Damköhler Number for diffusion, $N_D{}^{diff}$, is given by

$$N_D^{diff} = \frac{\tau\, K_R\, \alpha\, l^2}{\varphi\, D\, \mathrm{Ca}_{eq}} \tag{12}$$

For the parameters given above and l > 0.25 mm, $N_D{}^{diff}$ > 10, the condition for reaction to be fast compared with diffusion (e.g. Bickle, 1992). This short transport distance is consistent with the experimental observation that calcite dissolution experiments are transport controlled at pH < 5 (Pokrovsky et al., 2009) and implies that, while calcite is present in the reservoir, fluids will be close to equilibrium with calcite where CO_2 is transported by diffusion.

For advective displacements, transport and reaction may be described by

$$\varphi\frac{\partial \mathrm{Ca}}{\partial t} = -\varpi\varphi\frac{\partial \mathrm{Ca}}{\partial x} + K_R\alpha\left(1 - \mathrm{Ca}/\mathrm{Ca}_{eq}\right) \tag{13}$$

where ϖ is the net fluid pore velocity. Non-dimensionalising Eq. (13) using Eqs. (8) and (9) but with time scaled as

$$t = t'\frac{l}{\varpi\varphi} \tag{14}$$

transforms Eq. (13) to

$$\frac{\partial \mathrm{Ca}'}{\partial t'} = -\frac{\partial \mathrm{Ca}'}{\partial x'} + N_D(1 - \mathrm{Ca}') \tag{15}$$

where the Damköhler Number for advection, $N_D{}^A$ is given by

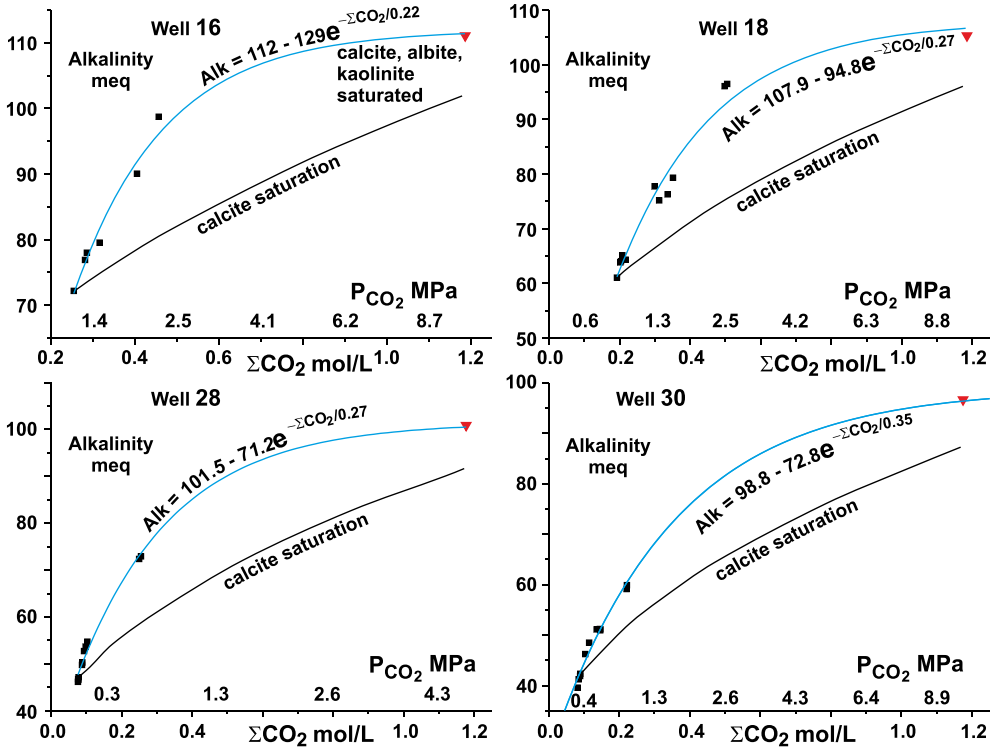


Fig. 17. Variation of alkalinity with total dissolved CO_2 (ΣCO_2) for fluids from wells (points give average of groups of 5 samples) where total CO_2 is calculated from assumption that fluids are in equilibrium with calcite at reservoir pressure of 10 MPa and temperature of 50 °C. Lines labelled 'calcite saturation' show evolution of initial fluid (average of first five samples) as CO_2 partial pressure is increased while maintaining equilibrium with only calcite. Red triangle shows alkalinity of initial fluid brought to equilibrium with calcite, albite and kaolinite. Calculated using PHREEQC. Blue lines are best fit to well sample alkalinity data with calcite-albite-kaolinite saturated composition fixing high ΣCO_2 end of line. (For interpretation of the references to color in this figure legend, the reader is referred to the web version of this article.)

$$N_D^A = \frac{K_R \alpha l}{\mathrm{Ca}_{eq} \varpi \varphi} \tag{16}$$

The maximum brine velocities at Salt Creek are ~5 m/day given the permeabilities (Fig. 4), driving pressure gradients (Fig. 5) and for the viscosity of supercritical CO_2 and therefore $N_D^A > 10$ for $l > \sim 5$ mm. Therefore fluids will approach saturation with calcite after flowing only 5 mm.

The conclusion is that on the length and velocity scales of the Salt Creek experiment transport rates are sufficiently slow that the fluids should remain close to equilibrium with calcite where calcite is present. It is therefore possible to estimate minimum fluid CO_2 contents and pH at reservoir conditions from the fluid chemistries and alkalinities presuming that calcite precipitation is limited as the fluids decompress in the production wells.

4.2. Alkalinity as a function of P_{CO_2} at calcite saturation

Fig. 17 illustrates the variation in alkalinity calculated using PHREEQC as a function of total CO_2 and P_{CO_2} for the fluids from wells 16, 18, 28 and 30 assuming that the fluids were in equilibrium with calcite at a reservoir pressure of 10 MPa and temperature of 50 °C. Also shown is the theoretical increase in alkalinity if the initial fluid sample (average of first 5 samples) is reacted only with calcite as the CO_2 partial pressure is increased. The deviation from the simple calcite saturation line is a consequence of the dissolution of silicate components in addition to calcite consistent with the modelling of the fluid compositions discussed above. This reduces the inferred CO_2 contents over those predicted from the increase in alkalinity being due to dissolution only of calcite.

One approximation with the use of the empirical curves calculated by fits to the sampled waters to calculate the expected alkalinity as a function of dissolved CO_2, is that the sampled waters are averages of the well waters over the whole depth of the 2nd Wall Creek which will range from CO_2-saturated to unaffected by the newly injected CO_2. The sampled waters therefore are restricted to lower dissolved CO_2 contents and alkalinities than the full range. The relationship between alkalinity and dissolved CO_2 will depend on the chemistry of these more saturated waters. A possible upper bound is shown by the alkalinity of the initial fluid brought to equilibrium with calcite, albite and kaolinite (Fig. 17). It should also be noted that mixing of fluids with the observed non-linear alkalinity-total CO_2 trends likely results in the mixture becoming undersaturated in calcite and/or silicate minerals.

4.3. Magnitude and kinetics of fluid-mineral reactions

The modal calculations (Fig. 12) indicate that the sampled fluids dissolve about 20 mmol plagioclase per litre on average over the 150 day sampling period. Again it is important to note that this is an average of all the fluids sampled which will range from those unreacted to those with most reaction, albeit biased towards the latter. An 'average' dissolution rate for the silicate minerals may be calculated given estimates of their surface areas, the porosity and the duration of the alteration. Surface areas of plagioclase measured by gas absorption (BET), are ~1 m^2/g. The porosity of the more permeable layers is ~20% and the plagioclase mode in Frontier Formation samples is ~15% by volume (e.g. Dutton et al., 2000). These parameters give a mean dissolution rate over the 150 days of injection of $\sim 10^{-12}$ $mol \cdot m^{-2} \cdot s^{-1}$. The major uncertainty is the estimate of plagioclase surface area for which 90% of the published measurements vary by a factor of 5 (see compilation in White and Brantley, 2003) and generally increase as dissolution reactions progress. The rate of 10^{-12} $mol \cdot m^{-2} \cdot s^{-1}$ is at the lower end of the range of far-from-equilibrium rates determined by many laboratory experiments at surface conditions. The 2nd Wall Creek Formation at Salt Creek has a temperature of ~50 °C which would increase plagioclase dissolution rates by a factor of ~7 over rates at 25 °C given an activation energy of ~60 $kJ \cdot mol^{-1}$ as estimated by Hellmann and Tisserand (2006) and Gruber et al. (2016). The compilation of plagioclase dissolution rates measured in laboratory experiments by White and Brantley (2003), adjusted to 50 °C, range from 2.5×10^{-12} to 10^{-10} $mol \cdot m^{-2} \cdot s^{-1}$. Gruber et al. (2016) measured dissolution rate of albite at 6×10^{-12} $mol \cdot m^{-2} \cdot s^{-1}$ at 50 °C.

It is of interest to estimate the CO_2 partial pressures necessary for

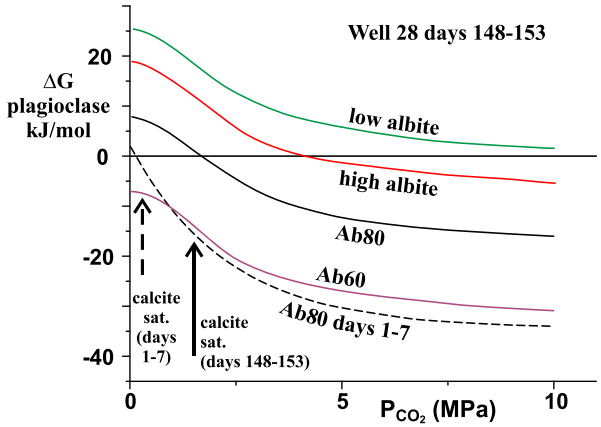


Fig. 18. ΔG for the plagioclase dissolution reaction calculated for Ab_{100}, Ab_{80} and Ab_{60} high albite and low albite (see Eqs. (17) & (18)) at a temperature of 50 °C and pressure of 10 MPa as a function of CO_2 partial pressure for the average brine sample from days 148 to153 from well 28. This sample is calcite saturated at a PCO_2 of 1.5 MPa (solid arrow). Dashed line shows ΔG for plagioclase Ab_{80} for the initial brine sample (days 1–7) which is calcite saturated at PCO_2 of 0.26 MPa (dashed arrow).

the plagioclase to be 'far-from-equilibrium' generally taken as ΔG for the plagioclase dissolution reaction of less than ~ < − 50 kJ/mol. The extent of thermodynamic disequilibrium between plagioclase and the average fluid sampled over days 148 to 153 from well 28 is illustrated in Fig. 18 as a function of the CO_2 partial pressure for low albite, high albite and high albite feldspar solid solutions with 20% and 40% anorthite. The deviation from equilibrium, ΔG in kJ/mol is given by (e.g. Drever, 1997)

$$\Delta G = RT \ln\left(\frac{IAP}{K_{eq}}\right) \tag{17}$$

where R is the gas constant, T temperature (K), IAP is the ion activity product and K_{eq} is the equilibrium constant for the plagioclase dissolution reaction

$$Na_xCa_{(1-x)}Al_{(2-x)}Si_{(2+x)}O_8 + 2(2-x).\ H^+ + (2x+4).\ H_2O = x.\ Na^+ + (1-x).\ Ca^{2+} + (2-x).\ Al(OH)_2^+ + (2+x).\ H_4SiO_4 \tag{18}$$

where x is the mol fraction albite. The equilibrium constant, K_{eq}, is calculated using the software package SUPCRTBL (Zimmer et al., 2016), an updated version of SUPCRT92 (Johnson et al., 1992). The thermodynamic properties of plagioclase solid-solutions are taken from Arnorsson and Stefansson (1999). The ion activity product is calculated using PHREEQC (version 3.3.8) with the PHREEQC data base and the thermodynamic properties of Al-species taken from Tagirov and Schott (2001). It is of interest that the calculated activities of Al-fluoride species in the brines become dominant at the reservoir conditions. For example in the 148–153 fluid from well 28 the calculated activity of $Al(OH)_2^+$ is $\sim 1.6 \times 10^{-7}$ at surface conditions decreasing to $\sim 2 \times 10^{-8}$ at a CO_2 pressure of 10 MPa. In contrast the activity of AlF_2^+ increases from $\sim 2 \times 10^{-9}$ at surface conditions to $\sim 3 \times 10^{-6}$ at 10 MPa CO_2 pressure.

The mean plagioclase composition from the core samples is ~An 21% (Table 1) and of the outcrop samples ~ An 15% (from Na/Ca ratios) and such plagioclases are just saturated (ΔG ~ 0) at calcite saturation in the well 28 samples (initial and final sample illustrated in Fig. 18). The more marked degrees of undersaturation illustrated in Fig. 18, required to drive plagioclase dissolution at the inferred rate implies higher CO_2 partial pressures at which calcite would also be undersaturated. However the uncertainties in the thermodynamic data are not well constrained and comparison of the different data sets PHREEQC.dat and lnll.dat with and without modified Al species gives a range of the order ± 8 kJ/mol for plagioclase. This, coupled with the uncertainties in plagioclase surface areas and plagioclase dissolution rates means that it is not possible to make a definitive conclusion as to the apparent discrepancy between CO_2 partial pressures inferred from calcite saturation and plagioclase dissolution rates. Alternatively it is possible that the brines precipitate significant carbonate on decompression or that the brines may be undersaturated in calcite because the rocks are heterogenous and some of the flow paths are calcite free (c.f. Fig. 13).

5. Conclusions

Sampling of fluids from sites where CO_2 is injected for enhanced oil recovery enables evaluation of fluid-rock interactions, rates of CO_2 dissolution in the sampled brines and gives a measurement of the heterogeneity of the formations sampled. The sampling of brines from production wells for six months after commencement of a phase of CO_2 injection into the 2nd Wall Creek member at the Salt Creek oil field, Wyoming, reveals marked increases in the concentrations of major cations over weeks, highlighting the reactivity of the relatively immature sandstone to CO_2-rich fluids. The concentrations of the anions Cl and Br remained unchanged which implies that the changes do not reflect heterogeneity in previously injected waters. Marked decreases in F during the sampling may reflect the volatility of SiF_4 which partitions into the CO_2 phase. Modelling the mineral reactions from the changes in cation chemistry indicates that mineral dissolution is dominated by plagioclase, with subsidiary biotite, calcite and chlorite. The silicate mineral dissolution is buffered by precipitation of the clay minerals.

The increase in Sr and $^{87}Sr/^{86}Sr$ ratios with time in the sampled fluids is consistent with the bulk of the Sr being supplied from plagioclase with elevated $^{87}Sr/^{86}Sr$ ratios and confirms the importance of dissolution of silicate minerals over the relatively short timescale in this experiment. The calculated $^{87}Sr/^{86}Sr$ ratios (0.7106 to 0.7156) of the silicate inputs lie within the range of the $^{87}Sr/^{86}Sr$ ratios (0.708 to 0.720) measured in the silicate fractions of core and outcrop samples from the Frontier Formation. The range of Sr-isotopic ratios across the different production wells demonstrates that flow paths within the reservoir sample horizons with distinct isotopic compositions, a conclusion consistent with the strongly heterogeneous permeabilities within the formation coupled with the marked Sr-isotopic heterogeneities. The chemical and isotopic variations in the time series from well 30 imply arrival of fluids from a different flow path with different extents of mineral-fluid reactions part way through the sampling period. These results attest to the sensitivity of geochemical tracers to flow paths and their variations, at least in formations with suitably reactive mineral assemblages.

The calculated rates of diffusion of CO_2 into brines and advection of CO_2 by flow rates within the formation are sufficiently slow that the fluids are expected to remain close to equilibrium with calcite, given its presence in the reservoir (calcite saturation is predicted after CO_2-enriched fluids migrated 5 mm into the reservoir). This allows estimation of the CO_2 contents of the fluids in the formation prior to their ascent and degassing in the production wells before sampling. Another potential constraint on the reservoir fluid CO_2 contents is the observation that the average rate of plagioclase dissolution is $\sim 10^{-12}$ mol·m^{-2}·s^{-1} (with uncertainty in plagioclase surface area of ~ a factor of five). This dissolution rate is relatively fast, especially considering that the sampled fluids represent an average of all fluids from the production well. These will range from those close to injected CO_2 and correspondingly CO_2-rich to those distant from penetrating CO_2 fingers and thus unsaturated, albeit that the sampling will be biased by the higher fluxes from the more permeable horizons adjacent to the CO_2 fingers. Formation CO_2 partial pressures in samples from the end of the sampling period estimated to drive the plagioclase dissolution at rates of 10^{-12} mol·m^{-2}·s^{-1} (with far-from-equilibrium rates of $\sim 1.6 \times 10^{-12}$ mol·m^{-2}·s^{-1}) are ~5 MPa compared with about

1.5 MPa for calcite saturation. However the combined uncertainties in plagioclase dissolution rates, plagioclase surface areas and the other model assumptions make the cause or even existence of this discrepancy uncertain.

The results attest to the utility of geochemical observations on CO_2 injection experiments to reflect reservoir structure and hydrological controls on the flow of CO_2 and brines. Dissolution of CO_2 in formation waters is probably the most importance longer-term stabilising mechanism in geological carbon storage. Targeted sub-surface sampling of fluids at reservoir conditions will be needed to confirm the rates of CO_2 dissolution and how these rates are impacted by reservoir heterogeneities.

Acknowledgements

We thank Anadarko for giving us access to samples and data from the Salt Creek field, Paul Hannah for providing sample processing facilities in Casper, logistic support and telemetry from the Salt Creek field during injection of noble gas spikes, Chen Zhu (Indiana) for updating the SupcrtBL data set spronsbl.dat with Al-F species, Vicki Stamp at RMOTC for facilitating fluid sampling at Teapot Dome and the USGS Denver core store for core from Salt Creek. The work was supported by the UK Natural Environment Research Council grants (CRIUS consortium NE/F004699/1 and Highlight grant NE/N016084/1) and the UK department of Energy and Climate Change.

Appendix A. Supplementary data

Supplementary data to this article can be found online at http://dx.doi.org/10.1016/j.chemgeo.2017.07.031.

References

Aagaard, P., Helgeson, H.C., 1982. Thermodynamic and kinetic constraints on reaction rates among minerals and aqueous solutions, I. Theoretical considerations. Am. J. Sci. 282, 237–285.
Arnorsson, S., Stefansson, A., 1999. Assessment of feldspar solubility constants in water in the range 0° to 350 °C at vapour saturation pressures. Am. J. Sci. 299, 173–209.
Benson, S.M., Cole, D.R., 2008. CO_2 sequestration in deep sedimentary formations. Elements 4, 325–331.
Bhattacharya, J.P., Willis, B.J., 2001. Lowstand deltas in the Frontier Formation, Powder River basin, Wyoming: implications for sequence stratigraphic models. AAPG Bull. 85, 261–294.
Bickle, M.J., 1992. Transport mechanisms by fluid-flow in metamorphic rocks: oxygen and strontium decoupling in the Trois Seigneurs massif — a consequence of kinetic dispersion? Am. J. Sci. 292, 289–316.
Bickle, M.J., 2009. Geological carbon storage. Nat. Geosci. 2, 815–818.
Bickle, M.J., Bunbury, J., Chapman, H.J., Harris, N.B., Fairchild, I.J., Ahmad, T., 2003. Fluxes of Sr into the headwaters of the Ganges. Geochim. Cosmochim. Acta 67, 2567–2584.
Bickle, M.J., Tipper, E.D., Galy, A., Chapman, H.J., Harris, N.W.B., 2015. On discrimination between carbonate and silicate inputs to Himalayan rivers. Am. J. Sci. 315, 120–166.
Boait, F.C., White, N.J., Bickle, M.J., Chadwick, R.A., Neufeld, J.A., Huppert, H.E., 2012. Spatial and temporal evolution of injected CO_2 at the Sleipner Field, North Sea. J. Geophys. Res. 117.
Drever, J.I., 1997. The geochemistry of natural waters, 3rd ed. Prentice Hall, Upper Saddle River (436 pp).
Dubacq, B., Bickle, M.J., Wigley, M., Kampman, N., Ballentine, C.J., Sherwood Lollar, B., 2012. Noble gas and carbon isotopic evidence for CO_2-driven silicate dissolution in a recent natural CO_2 field. Earth Planet. Sci. Lett. 341-344, 10–19.
Dutton, S.P., Willis, B.J., White, C.D., Bhattacharya, J.P., 2000. Outcrop characterization of reservoir quality and interwell-scale cement distribution in a tide-influenced delta, Frontier Formation, Wyoming, USA. Clay Miner. 35, 95–105.
Dutton, S.P., White, C.D., Willis, B.J., Novakovic, D., 2002. Calcite cement distribution and its effect on fluid flow in a deltaic sandstone, Frontier Formation, Wyoming. AAPG Bull. 86, 2007–2021.
Estabrook, E.L., 1925. Analyses of Wyoming oil-field waters. AAPG Bull. 9, 235–246.
Garçon, M., Chauvel, C., France-Lanord, C., Limonta, M., Garzanti, E., 2014. Which minerals control the Nd–Hf–Sr–Pb isotopic compositions of river sediments? Chem. Geol. 364, 42–45.
Gruber, C., Kutuzov, I., Ganor, J., 2016. The combined effect of temperature and pH on albite dissolution rate under far-from-equilibrium conditions. Geochim. Cosmochim. Acta 186, 154–167.
Hellmann, R., Tisserand, D., 2006. Dissolution kinetics as a function of the Gibbs free energy of reaction: an experimental study based on albite feldspar. Geochim. Cosmochim. Acta 70, 364–383.
Hovorka, S.D., Meckel, T.A., Trevino, R.H., Lu, J., Nicot, J.-N., Choi, J.-W., Freeman, D., Cook, P., Daley, T.M., Ajo-Franklin, J.B., Freifeild, B.M., Doughty, C., Carrigan, C.R., La Brecque, D., Kharaka, Y.K., Thordsen, J.J., Phelps, T.J., Yang, C., Romanak, K.D., Zhang, T., Holt, R.M., Lindler, J.S., Butsch, R.J., 2011. Monitoring a large volume CO_2 injection: year two results from SECARB project at Denbury's Cranfield, Mississippi, USA. Energy Procedia 4, 3478–3485.
IPCC, 2005. In: Metz, B., Davidson, O., de Coninck, H.C., Loos, M., Meyer, L.A. (Eds.), IPCC Special Report on Carbon Dioxide Capture and Storage. Prepared by Working Group III of the Intergovernmental Panel on Climate Change. Cambridge University Press, Cambridge, UK and New York, NY, USA (442 pp).
Johnson, J.W., Oelkers, E.H., Helgeson, H.C., 1992. Supcrt92 — a software package for calculating the standard molal thermodynamic properties of minerals, gases, aqueous species, and reactions from 1-bar to 5000-bar and 0-degrees-C to 1000-degrees-C. Comput. Geosci. 18, 899–947.
Kampman, N., Bickle, M., Becker, J., Assayag, N., Chapman, H., 2009. Feldspar dissolution kinetics and Gibbs free energy dependence in a CO_2-enriched groundwater system, Green River, Utah. Earth Planet. Sci. Lett. 284, 473–488.
Kampman, N., Bickle, M.J., Wigley, M., Dubacq, B., 2014. Fluid flow and CO2–fluid–mineral interactions during CO_2-storage in sedimentary basins. Chem. Geol. 369, 22–50.
Kampman, N., Busch, A., Bertier, P., Snippe, J., Hangx, S., Pipich, V., Di, Z., Rother, G., Harrington, J.F., Evans, J.P., Maskell, A., Chapman, H.J., Bickle, M.J., 2016. Observational evidence confirms modelling of the long-term integrity of CO_2-reservoir caprocks. Nat. Commun. 7, 10. http://dx.doi.org/10.1038/ncomms12268.
Kent, J., Watson, G., Onstott, T., 1990. Fitting straight lines and planes with an application to radiometric dating. Earth Planet. Sci. Lett. 97, 1–17.
Lee, K., Zeng, X., McMechan, G.A., Howell, J.C.D., Bhattacharya, J.P., Marcy, F., Olariu, C., 2005. A GPR survey of a delta-front reservoir analog in the Wall Creek Member, Frontier Formation, Wyoming. AAPG Bull. 89, 1139–1155.
Lee, K., Gani, M.R., McMechan, G.A., Bhattacharya, J.P., Nyman, S.L., Zeng, X., 2007. Three-dimensional facies architecture and three-dimensional calcite concretion distributions in a tide-influenced delta front, Wall Creek Member, Frontier Formation, Wyoming. AAPG Bull. 91, 191–214.
Lichtner, P.C., 1988. The quasi-stationary state approximation to coupled mass transport and fluid rock interaction in a porous medium. Geochim. Cosmochim. Acta 52, 143–165.
Lico, M.S., Kharaka, Y.K., Carothers, W.W., Wright, V.A., 1982. Methods of collection and analysis of geopressured geothermal and oil field waters. In: United States Geological Survey Water Supply Paper 2194, (21 pp).
May, S.R., Gray, G.G., Summa, L.L., Stewart, N.R., Gehrels, G.E., Pecha, M.E., 2013. Detrital zircon geochronology from Cenomanian–Coniacian strata in the Bighorn Basin, Wyoming, U.S.A.: implications for stratigraphic correlation and paleogeography. Rocky Mt Geol. 48, 41–61.
Merewether, E.A., Cobban, W.A., Cavaaugh, E.T., 1979. Frontier Formation and equivalent rocks in Eastern Wyoming. Mt. Geol. 16, 67–101.
Neufeld, J.A., Hesse, M.A., Riaz, A., Hallworth, M.A., Tchelepi, H.A., Huppert, H.E., 2010. Convective dissolution of carbon dioxide in saline aquifers. Geophys. Res. Lett. 37, L22404. http://dx.doi.org/10.21029/22010GL044728.
O'Brien, J., Moran, J., Wilbourn, G., Morris, S., Andersen, J., 2010. Monitoring a CO_2 flood with fine time steps: Salt Creek 4D. Lead. Edge 29, 912–919.
Parkhurst, D.L., Appelo, C.A.J., 2013. Description of input and examples for PHREEQC version 3—a computer program for speciation, batch-reaction, one-dimensional transport, and inverse geochemical calculations. In: U.S. Geological Survey Techniques and Methods. book 6 USGS (497 pp).
Pokrovsky, O.S., Golubev, S.V., Schott, J., Castillo, A., 2009. Calcite, dolomite and magnesite dissolution kinetics in aqueous solutions at acid to circumneutral pH, 25 to 150 °C and 1 to 55 atm pCO_2: new constraints on CO_2 sequestration in sedimentary basins. Chem. Geol. 265, 20–32.
Roberts, S., 1989. Wyoming Geomaps. Wyoming State Geological Survey Educational Series 1. (41 p).
Saffman, P.G., Taylor, G., 1958. The penetration of a fluid into a porous medium or Hele-Shaw cell containing a more viscous liquid. Proc. R. Soc. London, Ser. A 245, 312–329.
Tagirov, B., Schott, J., 2001. Aluminum speciation in crustal fluids revisited. Geochim. Cosmochim. Acta 65, 3965–3992.
de Villiers, S., Greaves, M., Elderfield, H., 2002. An intensity ratio calibration method for the accurate determination of Mg/Ca and Sr/Ca of marine carbonates by ICP-AES. Geochem. Geophys. Geosyst. 3. http://dx.doi.org/10.1029/2001GC000169.
White, A., Brantley, S., 2003. The effect of time on the weathering of silicate minerals: why do weathering rates differ in the laboratory and field? Chem. Geol. 202, 479–506.
Worden, R.H., Smith, L.K., 2004. Geological sequestration of CO_2 in the subsurface: lessons from CO_2 injection enhanced oil recovery projects in oilfields. Geol. Soc. Lond., Spec. Publ. 233, 59–85.
Xu, T., Apps, J., Pruess, K., Yamamoto, H., 2007. Numerical modeling of injection and mineral trapping of CO_2 with H_2S and SO_2 in a sandstone formation. Chem. Geol. 242, 319–346.
Young, H.W., Estabrook, E.L., 1925. Waters of the Salt Creek field, Wyoming. Trans. AIME G-25, 255–264.
Zhou, Z., Bickle, M., Galy, A., Chapman, H., Kampman, N., Dubacq, B., Wigley, M., Warr, O., Sirikitputtisak, T., Hannah, P., Ballentine, C., 2011. Predicting CO_2 EOR and geological sequestration processes with artificial noble gas tracers. Mineral. Mag. 75, 2274.
Zimmer, K., Zhang, Y., Lu, P., Chen, Y., Zhang, G., Dalkilic, M., Zhu, C., 2016. SUPCRTBL: a revised and extended thermodynamic dataset and software package of SUPCRT92. Comput. Geosci. 90, 97–111.